NASA TECHNICAL NOTE

NASA TN D-7066

NASA TN D-7066

EVALUATION OF AN AEROELASTIC MODEL TECHNIQUE FOR PREDICTING AIRPLANE BUFFET LOADS

by Perry W. Hanson

Langley Research Center
Hampton, Va. 23365

NATIONAL AERONAUTICS AND SPACE ADMINISTRATION • WASHINGTON, D. C. • FEBRUARY 1973

1. Report No.	2. Government Accession No.	3. Recipient's Catalog No.
NASA TN D-7066		

4. Title and Subtitle	5. Report Date
EVALUATION OF AN AEROELASTIC MODEL TECHNIQUE FOR PREDICTING AIRPLANE BUFFET LOADS	February 1973
	6. Performing Organization Code
7. Author(s)	8. Performing Organization Report No.
Perry W. Hanson	L-8460
	10. Work Unit No.
9. Performing Organization Name and Address	501-22-04-01
NASA Langley Research Center Hampton, Va. 23365	11. Contract or Grant No.
	13. Type of Report and Period Covered
12. Sponsoring Agency Name and Address	Technical Note
National Aeronautics and Space Administration Washington, D.C. 20546	14. Sponsoring Agency Code

15. Supplementary Notes

16. Abstract

A wind-tunnel technique which makes use of a dynamically scaled aeroelastic model to predict full-scale airplane buffet loads during buffet boundary penetration is evaluated. A 1/8-scale flutter model of a fighter airplane with remotely controllable variable-sweep wings and trimming surfaces was used for the evaluation. The model was flown on a cable-mount system which permitted high lift forces comparable to those in maneuvering flight. Bending moments and accelerations due to buffet were measured on the flutter model and compared with those measured on the full-scale airplane in an independent flight buffet research study. It is concluded that the technique can provide valuable information on airplane buffet load characteristics not available from any other source except flight test.

17. Key Words (Suggested by Author(s))	18. Distribution Statement
Buffet Aeroelasticity Damping Structural response Separated flow	Unclassified – Unlimited

19. Security Classif. (of this report)	20. Security Classif. (of this page)	21. No. of Pages	22. Price*
Unclassified	Unclassified	60	$3.00

*For sale by the National Technical Information Service, Springfield, Virginia 22151

EVALUATION OF AN AEROELASTIC MODEL TECHNIQUE FOR PREDICTING AIRPLANE BUFFET LOADS

By Perry W. Hanson
Langley Research Center

SUMMARY

A wind-tunnel technique which makes use of a dynamically scaled aeroelastic model to predict full-scale airplane buffet loads during buffet boundary penetration is evaluated. A 1/8-scale flutter model of a fighter airplane with remotely controllable variable-sweep wings and trimming surfaces was used for the evaluation. The model was flown on a cable-mount system which permitted high lift forces comparable to those in maneuvering flight. Bending moments and accelerations due to buffet were measured on the flutter model and compared with those measured on the full-scale airplane in an independent flight buffet research study. It is concluded that the technique can provide valuable information on airplane buffet load characteristics not available from any other source except flight test.

INTRODUCTION

Buffeting is the term loosely applied to the randomly fluctuating aerodynamic forces produced by separated flow or to the aeroelastic response of a structure to these forces. Buffeting of transport-type airplanes is of concern primarily with regard to onset conditions and shallow penetration of the compressibility buffet boundary due to upset conditions since this type airplane is not designed for high load factors. The concern is more for unpleasant vibrations and degradation of performance than for structural failure. Highly maneuverable high performance fighters, on the other hand, are subject to buffet flow due to shock—boundary-layer interaction, high angle of attack, and wake impingement. They are typically flown well into the buffet boundary where the buffet loads and accelerations build up rapidly with penetration. It has generally been found that even for these conditions, wing buffet loads are not the critical consideration but rather (1) vibrations which subject fire control, navigation and reconnaissance equipment, instruments, and crew to a more severe operational environment and increase fatigue; (2) degradation of performance through increased drag and decreased lateral stability which detracts from tracking capability; and (3) excessive structural loads on tail control surfaces. With regard to item (3) the horizontal tail is normally considered to be the critical tail compo-

nent for buffet loads. However, during recent wind-tunnel buffet studies on a fighter airplane, it was found that the critical components at high angles of attack were the vertical tails which were vibrating primarily in a torsion mode.

Although wing buffet phenomena have received much attention from investigators (refs. 1 to 8, for example), the ability to predict analytically the intensity of the buffet response as the buffet boundary is penetrated leaves much to be desired, and the ability to predict empennage buffet loads in turbulent wake flow is nonexistent. Although attempts are made during design to estimate buffet loads from past experience on similar configurations and from empirical means, the fact that buffet response phenomena are highly dependent on configuration detail and involve complex patterns of flow separation has led to the use of wind-tunnel data as a primary tool in predicting buffet onset flight conditions and, to a lesser extent, buffet intensity levels.

There are two fundamentally different methods of predicting the buffet intensity from wind-tunnel measurements on models of new configurations: (1) measure buffet accelerations or stresses on a dynamically scaled aeroelastic model and (2) measure the pressure fluctuations on a nominally rigid model and then calculate the dynamic response when these pressures act on the flexible structure. Each method has its advantages and disadvantages, but in either case there is a dearth of correlation information with which to evaluate the accuracy of the methods to predict full-scale buffet loads quantitatively, particularly for tail surfaces and transonic flight conditions. Most correlation studies have dealt chiefly with buffet onset predictions for wing buffet or with the relative magnitude of buffet loads as the buffet boundary is penetrated (refs. 9 to 11, for example). Generally, the predictions of buffet onset boundaries from wind-tunnel tests have been reasonably successful (although the definitions of onset are quite varied). Load predictions from simplified models, however, have not been notably successful, with the possible fortuitous exception of wing buffet, and the literature reflects contradictory conclusions with regard to the several techniques.

From considerations of the many factors involved, it would seem that the use of a complete dynamically and elastically scaled wind-tunnel model having a minimum of mount restraint would offer the potential for the most accurate prediction of absolute loads on both wing and tail surfaces and dynamic accelerations as the buffet boundary is penetrated. Models designed to provide freedom-from-flutter validation of new airplane designs closely satisfy the requirements for this type of buffet model. However, in practice even with this technique there are factors that could possibly affect the accuracy of the data, such as Reynolds number, wind-tunnel-wall, and pitch-rate effects.

An investigation was undertaken to develop and evaluate this wind-tunnel technique for predicting loads and accelerations due to buffet. The study included an assessment of (1) modeling requirements, (2) suitable means of approximating high load factor flight

conditions, and (3) the complexity of complete vehicle structural response to buffet flow. The method was evaluated by comparing the scaled buffet bending moments and accelerations measured on a 1/8-scale flutter model of the variable-sweep fighter airplane with those measured in a flight buffet research program (ref. 12). The investigation was conducted in the Langley transonic dynamics tunnel in the high subsonic and transonic speed ranges.

SYMBOLS

Physical quantities in this paper are given in both the International System of Units (SI) and U.S. Customary Units. The measurements and calculations were made in U.S. Customary Units. Factors relating the two systems are presented in reference 13.

a	root-mean-square normal acceleration, g units (1g = 9.80665 m/sec^2)
b	characteristic length, m (ft)
C/C_{cr}	ratio of generalized damping coefficient to critical value of damping
C_N	normal-force coefficient, N/qS
$\Delta C_{p,rms}$	root-mean-square fluctuating pressure coefficient, $\Delta p/q$
Δp	root-mean-square fluctuation of pressure about the mean, N/m^2 (lb/in^2)
EI	bending stiffness, $N\text{-}m^2$ ($lb\text{-}in^2$)
$F(f)$	power spectrum of unsteady pressure coefficient, 1/Hz
f	frequency, Hz
$\sqrt{fF(f)}$	nondimensional form of value of power spectrum of unsteady pressures at particular frequency
GJ	torsional stiffness, $N\text{-}m^2$ ($lb\text{-}in^2$)
I	mass moment of inertia, $m\text{-}N\text{-}sec^2$ ($in\text{-}lb\text{-}sec^2$)
K_D	aerodynamic scale factor, $\rho_r V_r b_r{}^2 m_r \omega_{n,r}$

K_a	buffet acceleration scale factor, $b_r^2 k_r^{1/2} q_r m_r (C_T/C_{cr})_r^{1/2}$
K_σ	buffet bending-moment scale factor, $b_r^3 k_r^{1/2} q_r (C_T/C_{cr})_r^{1/2}$
k	reduced frequency, $b\omega/V$
M	Mach number
m	mass, kg (slugs)
N	total aerodynamic normal lifting force, N (lb)
q	dynamic pressure, $\frac{1}{2}\rho V^2$, N/m^2 (lb/ft^2)
S	wing panel reference area, 0.762 m^2 (8.2 ft^2) for model
V	free-stream velocity, m/sec (ft/sec)
η_o	any particular nondimensional station
Λ	sweep angle of leading edge of wing, deg
ρ	airstream density, kg/m^3 ($slugs/ft^3$)
σ	root-mean-square bending moment, m-N (in-lb)
ω	circular frequency, $2\pi f$, rad/sec

Subscripts:

A	airplane
a	aerodynamic
M	model
n	nth natural vibration mode, n = 1, 2, 3, . . .
r	ratio, airplane to model

s structural

T total

t extraneous or "tare" value

APPARATUS AND PROCEDURE

Wind Tunnel

This investigation was conducted in the Langley transonic dynamics tunnel. This tunnel has a 4.88-m-square (16-ft) test section with cropped corners and is a return-flow, variable-pressure, slotted-throat wind tunnel. It is capable of operation at stagnation pressures from about 1724 N/m^2 (1/4 lb/in^2) to slightly above atmospheric pressure and at Mach numbers up to 1.2. Mach number and dynamic pressure can be varied independently with either air or Freon-12 used as a test medium. Freon-12 was used in the present investigation. Stagnation temperature during the tests was approximately 48.8° C (120° F).

An important factor in model dynamic measurements in wind tunnels is the airflow unsteadiness which, if excessive, may unduly affect the accuracy of the results or even mask the model dynamic characteristics to be evaluated. The ideal level of flow unsteadiness is, of course, zero. However, all tunnels have some flow unsteadiness and the acceptable level is determined by the type of dynamic measurements and the desirability of other tunnel operating characteristics. A measure of the suitability of this wind tunnel for buffet studies is depicted in figure 1. Figure 1(a) shows the variation of empty-tunnel sidewall rms fluctuating pressure coefficient with Mach number for the maximum dynamic pressure capability of the tunnel. The levels are of the order of fluctuating pressures in a turbulent flat-plate boundary layer (0.005 to 0.008 for the Mach number range considered (high subsonic and transonic)). (See ref. 14, for example.) Reference 15 presents a summary of transonic wind-tunnel noise investigations that show the fluctuating pressures on the tunnel center line generally to be less than those at the walls. The fluctuating pressure levels shown in figure 1(a) may therefore be regarded as the probable upper limits likely to be encountered in the vicinity of the tunnel center line where the model was flown. These levels are generally quite low compared with the levels measured in the other tunnels summarized in reference 15. It is of interest however to consider the power spectra of these pressure fluctuations. Figure 1(b) presents criteria for examining the suitability of a wind tunnel for buffet research, which take into account the frequency content of the unsteady tunnel flow. The criteria are based on the measurement of fluctuating static pressure on the tunnel wall and the results from studies of several different models in several different wind-tunnel test sections having varying degrees of flow unsteadiness

(ref. 16). In the figure, the ordinate $\sqrt{fF(f)}$ is a nondimensional form of the value of the power spectrum at important natural frequencies of the model to be tested, where $F(f)$ is the power spectrum of unsteady pressure divided by the dynamic pressure squared and f is the frequency in Hz. Along the left-hand side of the figure are shown the degrees of adequacy of the tunnel (from ref. 16) for two categories of buffet: light buffet generally pertaining to low-aspect-ratio, highly swept, thin surfaces and heavy buffet pertaining to relatively high-aspect-ratio, unswept, thick surfaces and surfaces in wake flow. From the figure it may be seen that the tunnel would be rated from good to adequate for heavy buffet and adequate to marginal for light buffet in the most critical area of $M = 0.7$ to 0.9. The horizontal tail would be the component most susceptible to these "extraneous" forces on the model in this range.

Model and Support System

Model description.- The model used in this investigation was a 1/8-size dynamically scaled aeroelastic model of a variable-sweep-wing fighter airplane that was initially designed and fabricated by the airplane manufacturer for use in flutter studies in the Langley transonic dynamics tunnel on a cable-mount system. The required stiffness was provided by steel spars in the wing and fuselage while ballasted segmented sections made from balsa and fiber glass provided the required shape and mass. The horizontal and vertical tails were of a stressed skin type construction (etched aluminum skin on balsa cores). The horizontal-tail pitch deflection and wing sweep angle were remotely controllable and the horizontal tail could be differentially operated for roll control. Flow-through nacelles were incorporated, but mass flow through them was not simulated. The model was used successfully in flutter studies from the prototype phase to the present configuration and has undergone several updating changes. The only alteration made to the model for the buffet studies was the addition of strain gages and accelerometers at appropriate locations (see section "Instrumentation and Data Reduction") and a fitting for attaching the lift-balancing cable (see section "Lift-balancing device"). This model was designed to simulate a preprototype version of the fighter airplane and differs in some respects from the flight buffet test airplane. Although the model weight, center of gravity, and inertias compare favorably with the test airplane, the horizontal-tail pivot location on the test airplane is 0.127 m (5 in.) (full scale) forward of the model pivot location (less than 3-percent-root-chord difference). The model weighed 43.3 kg (95.5 lb) and had a full wing span of about 2.29 m (7.5 ft) at the 26° sweep position. Figure 2 is a photograph of the model suspended on the transonic dynamics tunnel cable-mount system while undergoing flutter studies. The external stores and mounts shown were removed for the buffet tests.

Model design scale factors.- The model was designed for a Mach number ratio of 1, and for a mass-density ratio scaling parameter of 1.0 at a full-scale airplane weight of

32 300 kg (71 200 lb), and a reduced velocity parameter of 0.837 (or, conversely, a reduced stiffness parameter of 1.195). The scale factors used in the model design were determined by wind-tunnel size, test medium, and tunnel performance capabilities and by the full-scale flight boundary.

The present model was designed originally as a flutter model to demonstrate that the airplane would have the required flutter safety margin. Such models may be designed to be tested at wind-tunnel conditions that are scaled from the airplane actual flight boundary which has been increased by the flutter safety margin, in which case, $k_{n,r} = 1$; or, they may be designed with the model stiffness reduced in proportion to the flutter safety margin requirements and then tested at wind-tunnel conditions that are scaled values of the airplane actual flight boundary.

The latter philosophy can alleviate practical problems in model fabrication by allowing the model to be less stiff for the same mass and was followed for the design of the present flutter model. Detailed discussion of dynamic aeroelastic model scaling theory is presented in reference 17. The basic design and derived scale factors are presented in table I.

Model vibration characteristics.- Some of the more important model natural vibration frequencies scaled to full-size airplane values are compared with airplane values in table II. These full-scale airplane values were measured on the first airplane by the manufacturer. The frequencies are almost the same as those given in reference 12 for the test airplane flown in the flight buffet tests. Model data were measured with the model suspended on very soft springs. The agreement between model and airplane values is considered to be very good. Although no attempt was made to control the model structural damping, the table shows that the model and airplane structural damping ratios were generally comparable.

Some of the model natural vibration mode shapes and frequencies of interest for the various wing sweep angles are shown in model scale in figure 3. All the vibration characteristics are given for the model ballasted to simulate the fuselage-full wing-empty fuel condition corresponding to an airplane weight of 32 300 kg (71 200 lb). The flight buffet data were measured on the test airplane with wing tanks empty, but the total airplane weight varied from about 33 600 to 26 300 kg (74 000 to 58 000 lb) due to usage of fuel from the fuselage tank. This weight variation would have the primary effect of changing the natural frequencies slightly.

Mount system.- For these tests the cable-mount system consisted of two cable loops. (See fig. 2.) A forward flying cable was reeved over pulleys in the model in the horizontal plane and secured to each tunnel sidewall about 9.14 m (30 ft) upstream of the model. The rear flying cable passed over pulleys in the model in the vertical plane and extended downstream of the model where one end was attached to the tunnel ceiling and

the other end was attached to a variable tensioning device through a soft spring. In addition, a snubber cable system was provided for emergency restraint. It consisted of three cables which were fastened to the model near the center of gravity and which extended out through the tunnel walls and ceiling to a shock absorber system and a remotely operable actuator. The snubber cables, shown taut in the photograph, are normally slack during data taking. The mount-system characteristics are described in more detail in reference 18.

The flexible umbilical is used to carry instrumentation leads and horizontal-tail and wing-sweep actuator motor power leads from the model.

Lift-balancing device.- Normally the cable-mount system allows the model to fly rather freely near the tunnel center line with the model trimmed to support its own weight. In order to fly the model under high load factor conditions, it was necessary to counteract the lift that was in excess of the model weight; this was accomplished by means of a lift-balancing cable which was attached to the model near the center of gravity (c.g.) and which extended downward through the tunnel floor to a load link and then to a lift-balancing device which is illustrated schematically in figure 4. The cable is attached to a blowby, low-friction piston in a cylinder connected to large pressure reservoir tanks and to a large exhaust buffer tank. The large volume pressure reservoirs provide a relatively constant low level spring rate which allows the model to respond in rigid and elastic body dynamic motions with a minimum of restraint. The static lift-balancing force exerted by the lightweight piston is controlled remotely by varying the air pressure acting on the piston. The load link measures the force being exerted on the model by the device which is capable of producing up to 6670 N (1500 lb) of force.

Instrumentation and Data Reduction

For the buffet studies the model was instrumented to measure dynamic bending moments and accelerations at locations nearly the same as those on the airplane as possible. Four-active-arm, resistance-wire, temperature-compensated, strain-gage bridges to measure the left and right horizontal-tail bending moments at the root chords were bonded to the horizontal-tail pivot shafts at the same location as on the airplane. Strain-gage bridges also were bonded to the right and left wing spars and oriented to measure bending moments at the same location as on the airplane (23.83 cm (9.38 in.), model scale, outboard of the wing pivot center measured along the 26-percent-chord line). Measurements were made only on the right wing of the airplane. An accelerometer to measure normal dynamic accelerations was located in the model at the nominal c.g. location. The normal accelerations were measured on the airplane at a point 15.88 to 19.05 cm (6.25 to 7.5 in.), model scale, forward of this location, although in reference 12 they are referred to as being nominally at the center of gravity. In addition, an accelerometer was located in the model to measure the dynamic normal accelerations at the pilot station.

Other measurements made during the study were model angle of attack, force on the lift-balancing cable, left and right horizontal-tail deflection angles, wing sweep angles, and wind-tunnel parameters.

Figure 5 is a schematic diagram of the signal conditioning and data-recording process. The signals from the model bending-moment strain gages and accelerometers were amplified by 3-kHz carrier amplifiers. The amplified signals were recorded on oscillographs for total load monitoring. They were also routed through 200-Hz low-pass filters to eliminate frequencies above the range of interest and through dc blocking capacitors to eliminate static bias to a 14-channel FM tape recorder. The dynamic portion of the signals was recorded at 9.53 cm/sec $\left(3\frac{3}{4}\text{ in./sec}\right)$ for later electronic analysis. The analog signals were converted to engineering units and digitized at a sampling rate of 500 samples/sec. Standard digital-computer random-process analysis techniques were used to generate power spectral densities and rms levels of the model response. The model data were analyzed over a frequency range from 3 to 150 Hz, with a frequency bandwidth of 3 Hz. (The airplane data of ref. 12 were analyzed to 50 Hz with a frequency bandwidth of 1 Hz.) The model data sample periods were approximately 30 sec, whereas the airplane data sample periods were 3 sec. Signals from the horizontal-tail and wing position indicators, model angle of attack servo accelerometer, lift-balancing cable load link, and tunnel pressure and temperature sensors were routed through digitizing potentiometers to a card punch. Test-point identification information served to correlate the tape-recorder data with the punch-card data.

From repeatability tests it is estimated that the maximum error of the wind-on measurements of model normal-force coefficients, dynamic bending moments, and dynamic accelerations was approximately ±5 percent; maximum error in angle of attack was approximately $\pm 1/2^{\circ}$. Tunnel flow parameters are generally accurate to less than ±1 percent except that the maximum error in Mach number is about ±1/2 percent.

Test Conditions and Procedures

Measurements were made on the model at tunnel conditions (Mach number and dynamic pressure) that simulated most of the full-scale flight conditions during the flight buffet measurements reported in reference 12. In the wind-tunnel tests the procedure was to stabilize the tunnel at a Mach number and dynamic pressure scaled from averaged values measured during the particular flight buffet test maneuver. The model was first flown at a given wing sweep angle on the cable-mount system just lifting its own weight. The horizontal tails were then positioned to produce discrete increments in model angle of attack. At each selected angle of attack a 30-sec tape data sample of model bending moments and accelerations was recorded, along with the tail positions, angle of attack, lift-balancing cable load, and tunnel conditions. The angle of attack was increased in increments until no further increase was possible either because maximum tail deflection

angles or maximum model design loads were reached, or because of model instability. The wing sweep angle was changed to a new setting and the procedure was repeated for the other sweep angles.

The model and airplane relative buffet onset boundaries and buffet boundary penetrations are compared in figure 6. The reasons for termination of the model penetrations are indicated in the figure.

Figure 7 compares the variations of the model normal-force coefficients with angle of attack with those of the airplane for various Mach numbers and wing sweep angles. For comparable test conditions the flight Reynolds numbers (based on the wing mean chord at 16^{o} sweep) varied from 2.2×10^6 to 3.1×10^6, whereas the model Reynolds numbers varied from 0.77×10^6 to 1.18×10^6. The model and airplane data are felt to compare favorably.

DATA ANALYSIS

Scaling Buffet Loads and Accelerations

For wind-tunnel buffet studies on models to be useful in predicting full-scale buffet loads, the necessary buffet response scaling relationships must be known. Over the years investigators have developed buffet scaling relationships that generally have been much simplified and oriented to the particular study at hand (refs. 4 and 5, for example). The complexity of these relationships depends on the complexity of the dynamic system involved. For a complete airplane structure the system is indeed quite complex and certain simplifying assumptions are required, such as considering components of the structure individually (wing, horizontal tail, etc.) in order to derive workable relationships. The development of buffet loads scaling relationships normally follows the method of generalized harmonic analysis. The method is treated in some length in reference 19 and was first applied to the analysis of buffeting in reference 1. One of the more general developments which considers distributed load and structural characteristics and discrete modal contributions to the total response is presented in reference 20. The development requires that the model frequency spectrum be reasonably representative of the full-scale vehicle, or at least be representative of the important vibration modes involved in the vehicle buffet response. Although the scaling relationships developed in reference 20 were derived for scaling launch vehicle buffet responses, they are applicable to any linear multi-degree-of-freedom system. They are used as a basis for buffet loads scaling in this study.

From equation (15) of the appendix of reference 20 the buffet bending-moment scaling relationship may be written in the present notation as

$$\sigma^2(\eta_o)_{T,A} = b_r{}^6 q_r{}^2 \sum_{n=1}^{\infty} k_{n,r} \left[\frac{\left(\frac{C_a}{C_{cr}}\right)_{n,M} + \left(\frac{C_s}{C_{cr}}\right)_{n,M}}{\left(\frac{C_a}{C_{cr}}\right)_{n,A} + \left(\frac{C_s}{C_{cr}}\right)_{n,A}} \right] \left[\hat{C}_{L,n}(k_n)\right]_r \sigma^2(\eta_o)_{n,M} \qquad (1)$$

where

$\sigma(\eta_o)_{T,A}$ airplane total root-mean-square buffet bending moment at a particular location

b_r airplane-to-model length ratio

q_r airplane-to-model dynamic pressure ratio

$k_{n,r}$ airplane-to-model reduced frequency ratio for nth natural vibration mode, $b_r\omega_{n,r}/V_r$

$\left[\hat{C}_{L,n}(k_n)\right]_r$ airplane-to-model ratio of power spectrum of effective random aerodynamic lift coefficient

$\sigma(\eta_o)_{n,M}$ model root-mean-square buffet bending moment in nth vibration mode at a particular location

$\left(\frac{C_a}{C_{cr}}\right)_{n,M} + \left(\frac{C_s}{C_{cr}}\right)_{n,M}$ sum of model aerodynamic and structural damping in nth vibration mode

$\left(\frac{C_a}{C_{cr}}\right)_{n,A} + \left(\frac{C_s}{C_{cr}}\right)_{n,A}$ sum of airplane aerodynamic and structural damping in nth vibration mode

An expression similar to equation (1) can be derived for the airplane root-mean-square buffet acceleration at a particular location

$$a^2(\eta_o)_{T,A} = b_r{}^4 q_r{}^2 \sum_{n=1}^{\infty} k_{n,r} \frac{1}{m_r{}^2} \left[\frac{\left(\frac{C_a}{C_{cr}}\right)_{n,M} + \left(\frac{C_s}{C_{cr}}\right)_{n,M}}{\left(\frac{C_a}{C_{cr}}\right)_{n,A} + \left(\frac{C_s}{C_{cr}}\right)_{n,A}} \right] \left[\hat{C}_{L,n}(k_n)\right]_r a^2(\eta_o)_{n,M} \qquad (2)$$

where

m_r airplane-to-model mass ratio

$a(\eta_o)_{n,M}$ model root-mean-square buffet acceleration in nth vibration mode at particular location

From equations (1) and (2) it can be seen that the total mean-square bending moment and acceleration is a superposition of single-degree-of-freedom responses, that is, the derivation treats each mode as a separate independent system with modal coupling neglected. Thus, the model/airplane scaling relationships are dependent on the structural and aerodynamic damping ratio, the reduced-frequency ratio of each vibration mode of interest, and the term $\left[\hat{C}_{L,n}(k_n)\right]_r$. Ideally, the reduced-frequency ratio should be unity in order that the effective aerodynamic lift coefficients of the model and airplane be identical.

Because of slight variations of the speed of sound in the wind tunnel with respect to the speed of sound in flight (the airplane tests were conducted at several altitudes) and because the present model was designed to demonstrate the required flutter margin by a reduction in stiffness, the actual reduced-frequency ratios varied from the optimum value of one by 25 to 37 percent. The actual values of the square root of the reduced-frequency ratios are shown in table III. These values are based on a frequency ratio ω_r approximately equal to 1/3 for all modes (determined from measured airplane and model frequencies). For the range of reduced frequencies of this study, these variations of k_r are considered to be negligible and the value of the term $\left[\hat{C}_{L,n}(k_n)\right]_r$ is assumed to be unity.

For dynamically scaled aeroelastic models with relatively low structural damping, the damping term in brackets in equations (1) and (2) will normally be very near unity. (See section "Modeling Considerations.") However, it was of interest to estimate the value of the term in the present study. The model structural damping $(C_s/C_{cr})_{n,M}$ and airplane structural damping $(C_s/C_{cr})_{n,A}$ were measured for the modes considered to be of primary importance in the buffet response. The model aerodynamic damping $(C_a/C_{cr})_{n,M}$ was calculated based on reference 21 since the flutter model used did not have sufficient instrumentation to measure aerodynamic damping in buffet flow. Calculated values of airplane aerodynamic damping were also used since no measured values were available from the flight buffet tests. The airplane aerodynamic damping can be related to the model aerodynamic damping by

$$\left(\frac{C_a}{C_{cr}}\right)_{n,A} = \left(\frac{\rho_r V_r b_r^2}{m_r \omega_{n,r}}\right)\left(\frac{C_a}{C_{cr}}\right)_{n,M} \tag{3}$$

(see ref. 21, for example) or

$$\left(\frac{C_a}{C_{cr}}\right)_{n,A} = K_D\left(\frac{C_a}{C_{cr}}\right)_{n,M} \tag{4}$$

where

$$K_D = \frac{\rho_r V_r b_r^2}{m_r \omega_{n,r}}$$

During flight flutter tests at $\Lambda = 26^o$, some limited measurements of the airplane aerodynamic damping in the wing bending mode were made. The measured airplane values of 0.77 to 0.82 agreed well with the calculated values of 0.75 to 0.94.

Since the frequency ratio is taken to be the same value for all modes of interest $(\omega_r = 1/3)$, the reduced-frequency ratio will be the same for all modes and equations (1) and (2) may be written as

$$\sigma^2(\eta_o)_{T,A} = b_r^6 q_r^2 k_r \sum_{n=1}^{\infty} \frac{1}{(C_T/C_{cr})_{r,n}} \sigma^2(\eta_o)_{n,M} \tag{5}$$

and

$$a^2(\eta_o)_{T,A} = b_r^4 q_r^2 k_r \frac{1}{m_r^2} \sum_{n=1}^{\infty} \frac{1}{(C_T/C_{cr})_{r,n}} a^2(\eta_o)_{n,M} \tag{6}$$

where

$$\left(\frac{C_T}{C_{cr}}\right)_{r,n} = \frac{\left(\frac{C_a}{C_{cr}} + \frac{C_s}{C_{cr}}\right)_{n,M}}{\left(\frac{C_a}{C_{cr}} + \frac{C_s}{C_{cr}}\right)_{n,A}}$$

Actually it is not generally possible to measure directly the bending-moment $\sigma(\eta_o)_{n,M}$ or acceleration $a(\eta_o)_{n,M}$ buffet response of the model in a particular mode. Rather, the total response at a particular location σ_M is measured and the "modal composition" of the indicated response is estimated from power spectra. Several conditions are inferred in this application of the scaling relationships: (1) The "natural vibration modes" of importance in the total response can be identified, are well separated, and are lowly damped; (2) the total measured model response can be treated as a summation of individual modal responses, that is, $\sigma_M^2 = \sum_{n=1}^{\infty} \sigma_{n,M}^2$; and (3) the structural and aerodynamic damping of the modes are known or can be estimated. Although condition (1) may not be strictly met for the horizontal tail and c.g. acceleration responses because in some cases the modes were not well separated, it was assumed that these responses came acceptably close to meeting this condition for application of the scaling relationships. Therefore, the airplane buffet response at a particular location can be determined by the modal summations indicated in equations (5) and (6). In practice, this may prove to be a difficult process. In the present case, the character of the responses and the fact that the model was a good dynamic representation of the airplane permitted some simplifications. The measured total wing bending-moment response (of both the model and the airplane) was very similar to that of a single-degree-of-freedom system with the response frequency equal to the wing first bending frequency. (See fig. 8(a).) In contrast, power spectra of the horizontal tail and c.g. accelerations (figs. 8(b) and 8(c)) reveal some energy at frequencies approximating those of several natural vibration modes. However, the model spectra generally indicated that the major portion of the total response was near frequencies corresponding to the horizontal tail bending, fuselage vertical bending, and wing first bending modes. Since the total damping ratios $(C_T/C_{cr})_{r,n}$ for each of these modes was very nearly the same (table III), it was expedient to assume that the damping associated with all the modes involved in the horizontal-tail total bending-moment response was that of the horizontal-tail bending mode. Similarly, the total damping ratio associated with the total c.g. acceleration response was considered to be that of the fuselage vertical bending mode.

Equations (5) and (6) are then simply

$$\sigma(\eta_o)_{T,A} = \sigma_A = K_\sigma \sigma_M \tag{7}$$

and

$$a(\eta_o)_{T,A} = a_A = K_a a_M \tag{8}$$

where

$$K_\sigma = b_r^3 k_r^{1/2} q_r \left(\frac{C_T}{C_{cr}}\right)_r^{-1/2} \tag{9}$$

$$K_a = b_r^2 k_r^{1/2} q_r m_r^{-1} \left(\frac{C_T}{C_{cr}}\right)_r^{-1/2} \tag{10}$$

and σ_M is the total rms buffet bending moment measured on the model wing or horizontal tail, a_M is the total rms buffet acceleration measured on the model at the c.g. and pilot station, and σ_A and a_A are the corresponding full-scale bending moments and accelerations. The total damping ratio $\left(C_T/C_{cr}\right)_r$ is that of the wing first bending mode, the horizontal-tail bending mode, or the fuselage vertical bending mode for wing, horizontal tail, or c.g. acceleration measurements, respectively. The values of the flow-related scaling ratios and scaling constants used in converting from model to full-scale values are shown in table III.

Extraction of Extraneous Response

Both the flight- and wind-tunnel-model dynamic loads and accelerations, as measured, are the result of both buffet and extraneous forces. The airplane instrumentation measures structural response to atmospheric turbulence, sudden actuator movements, and engine and auxiliary motor vibrations, in addition to the response of the structure to buffet flow. The model instrumentation measures response to tunnel turbulence and mounting cable vibrations in addition to the response to buffet flow. Generally these extraneous responses are relatively constant for a particular Mach number and dynamic pressure as angle of attack or normal force is varied and can be considered "tare" values to be subtracted from the total response. Figure 9 illustrates the manner in which the model tare values were determined. The total measured model and airplane dynamic bending moments and accelerations are shown as a function of normal-force coefficient. For comparison purposes, the total model response has been scaled to full-scale values. Figure 9(a) is typical of the model response for the 26° wing sweep condition for all Mach numbers and for the higher sweep angles at low Mach numbers. Figure 9(b) is more generally representative of the response at higher wing sweeps at the higher Mach numbers. The wing bending moments and c.g. accelerations are seen to increase only slightly until a certain value of C_N is reached, after which the level of response increases rapidly. This characteristic also is true for the horizontal-tail bending moments for the low wing

sweep conditions. Model buffet response is said to begin at the intersection of straight lines faired through the total response prior to and after buffet onset. The values of the accelerations or bending moments at this point are taken to be the tare values a_t or σ_t, respectively. For those instances where the horizontal-tail response did not exhibit a clear change in character, the tare values were determined by multiplying the relatively well-defined tare values at $M = 0.52$ by the ratio of the tunnel turbulence level at the Mach number in question to the level at $M = 0.52$ (as determined from fig. 1(b)). In most instances the tare values determined in this manner were approximately the same as the minimum values of bending-moment response observed over the range of C_N variation.

If there is no correlation between tunnel unsteadiness and the buffet response the actual model root-mean-square buffet bending moments σ_M are given by

$$\sigma_M = \left(\sigma_T^2 - \sigma_t^2\right)^{1/2} \tag{11}$$

where σ_T is the measured total rms bending moments.

Similarly, the model buffet accelerations a_M are given by

$$a_M = \left(a_T^2 - a_t^2\right)^{1/2} \tag{12}$$

where a_T is the measured total rms accelerations.

The measured airplane rms bending moments and accelerations given in reference 12 and shown normalized by airplane design values in figure 9 are total values. For the flight buffet studies extraneous nonbuffet related structural responses were considered to be insignificant since the flight data were purposely taken under minimal turbulence conditions. From unpublished data supplied by the authors of reference 12 and considered by them to be typical of prebuffet levels for all the flight data, it was concluded that for consistency in the model/flight comparisons the following small tare values would be appropriate:

Measurement	Prebuffet tare values, percent design
rms wing bending moment (right)	0.112
rms horizontal-tail bending moment:	
Left	0.147
Right	0.158
rms acceleration at c.g.	0.177

These nonbuffet related values were subtracted from the total airplane values presented in reference 12 in the same manner as for the model data. Buffet onset on the airplane was said to occur when the peak-to-peak c.g. accelerations exceeded approximately 0.8 percent of the design load factor.

It may be noted that the mathematical procedure required to separate the nonbuffet related response from the total (taking the square root of the difference of squares) results in tare values having a minimum effect at the higher values of total response where the greater interest lies for predicting buffet loads.

Figure 9 also illustrates an unfortunate aspect of the flight buffet studies with regard to comparative evaluations, namely the low level of the buffet loads and accelerations due to the previously mentioned load-factor and angle-of-attack limitations that had been imposed on the preprototype airplane. The maximum dynamic component of the loads measured was generally not greater than 1 percent of design loads and the maximum acceleration response was generally little greater than 2 percent of design load factor. These low levels result in a rather severe test of the buffet loads prediction capability of the present method due to the relatively larger values of extraneous response and effects over which the investigator has little or no control.

DISCUSSION OF AEROELASTIC MODEL TECHNIQUE

Some of the more important modeling considerations, including compromises, necessary to evaluate effects of buffet flow are discussed and related to the buffet loads scaling relations. Model testing technique, including limitations, deficiencies, and potential impact on scaled results are then discussed.

Modeling Considerations

The goal, of course, is to subject a reduced size model that accurately reflects the shape and structural characteristics of the airplane to wind-tunnel flow that accurately simulates the airflow over the airplane and to support the model in the wind tunnel in a manner such that the model and airplane degrees of freedom and inertia forces are properly related. In practice, it is impossible to meet all these requirements, but a complete dynamically scaled aeroelastic model suspended on the cable-mount system described earlier comes reasonably close to meeting them. The model should be as large as possible, consistent with the tunnel test section size to facilitate model fabrication and, for buffet models, to provide a Reynolds number as large as possible. Buffet flow is influenced by the nature of the boundary layer which, of course, can be a function of Reynolds number. Because of wind-tunnel performance limitations, practical model fabrication considerations, and the overriding importance of testing the model at a mass-density

ratio comparable to that of the airplane, no attempt normally is made to simulate Reynolds number in high-speed flutter models. The same compromise would have to be made for high-speed buffet models. Another factor affecting the boundary layer which may be more important for buffet models than for flutter models is the skin surface smoothness. The model used in the present studies was of a "segmented pod" type construction which results in small surface discontinuities at the edges of the individual segments. However, the Reynolds number scale effects and surface roughness are believed primarily to influence the buffet onset boundary and residual model response prior to buffet onset rather than the load intensities once the buffet boundary has been penetrated. Figure 6 indicates that even the buffet onset conditions were predicted reasonably well except for the 72^{o} wing sweep condition and figure 7 shows that the variation of normal-force coefficient with angle of attack was essentially the same for the airplane and model. Although the locations of local shocks and commencement of separated flow may have been different for the model and airplane, their integrated effects on the structural response apparently were small.

Once the model size is selected, the stiffness and mass scale ratios remain to be determined. These ratios are a function of model size. The airplane flight conditions must be simulated (Mach number and altitude) within the wind-tunnel operational capabilities. For a Mach number ratio of 1 and a nominal ratio of airplane to tunnel speed of sound, the resulting density and velocity ratios determine the nominal mass and stiffness ratios. The model is then fabricated to obtain the scaled mass and stiffness distributions as closely as possible. The natural vibration mode shapes of the successful model will be very nearly the same as the airplane. If the measured node lines of the vibration modes of the model and the calculated or measured node lines of the airplane are very near the same location and if the scaled model frequencies are within a few percent of the desired value, the model is said to be satisfactory.

From equations (1) and (2) it is clear that the relationship between the total damping (structural plus aerodynamic) is as important in scaling buffet response as the stiffness and mass characteristics. For a properly scaled model tested at exactly the scaled flight conditions, the airplane aerodynamic damping $\left(C_a/C_{cr}\right)_{n,A}$ is related to the model aerodynamic damping $\left(C_a/C_{cr}\right)_{n,M}$ by the reciprocal of the reduced stiffness ratio k_r; therefore when $k_r = 1$, they are equal. (The aerodynamic damping scale factor K_D of eq. (4) differs from $1/k_r$ to account for off-design test conditions of the model used in the study.) If it could be arranged to have the model structural damping equal to that of the airplane for the various vibration modes, then the total damping ratio would be equal to 1. Unfortunately, modeling technology has not advanced to the point where this is possible and attempts to control model structural damping are usually limited to keeping the model structural damping to reasonably small fractions of critical damping or pro-

viding an artificial means of varying the structural damping over a limited range. This latter method was used in the damping studies of reference 22 to confirm the relationship between buffet bending moment and total damping coefficient

$$\sigma \approx \frac{1}{\left(C_T/C_{cr}\right)^{1/2}}$$

The measured structural damping coefficients of the model used in the present study were approximately the same as the airplane structural damping coefficients for the primary modes of interest (table II), and were roughly an order of magnitude smaller than the calculated model aerodynamic damping (table III). Since the aerodynamic scaling factor K_D did not vary by more than +5 percent and -14 percent from 1.0 for all the test conditions, the resulting total damping ratio for the present model has only a small effect on the bending moment and acceleration scaling factors K_σ and K_a. This situation is in contrast to the one where solid metal aerodynamic force models are used to estimate wing buffet loads. Although in some instances such models may have wing reduced frequencies approximately equal to those of the airplane when tested at suitable velocities, the model aerodynamic damping C_a/C_{cr} will be low due to the relatively large model mass $\left(C_{cr} = 2m\omega\right)$ so that the model structural damping coefficient is likely to predominate, whereas the airplane aerodynamic damping coefficient is likely to predominate except for flight conditions approaching flutter.

Even with the use of dynamically scaled aeroelastic models, certain simplifying assumptions are usually made. For the present studies, it was assumed that wind-on mode shapes were essentially the same as wind-off shapes and that there were no significant differences in model and airplane mode shapes that were important in the buffet response. It was also assumed that the model and airplane structural damping was constant; that is, the structural damping in a particular mode was independent of vibration amplitude, temperature, and flow conditions. In fact, the structural damping may vary with amplitude and temperature so that the accuracy of the method could be improved by incorporating in the model a means for measuring the total wind-on damping in the vibration modes of interest or by determining the total damping of the model response by consideration of the half-power point bandwidth of resonant peaks in the power spectra. (See ref. 23, for example.) If damping is to be determined in this manner, appropriate sampling rates and filter bandwidths must be used and spectrum analyzer characteristics must be accounted for. The technique was not used in the present study because the power spectra parameters (filter bandwidth, frequency range, etc.) were chosen to be compatible with the flight spectra for comparison purposes rather than for accuracy in determining model damping.

Testing Technique

A basic difference in the flight and wind-tunnel buffet studies was the manner in which the structure was introduced to buffeting flow. The model angle of attack was slowly increased at essentially constant flow conditions and the response measurements were made at a constant angle of attack, whereas the airplane approached buffeting in maneuvering flight with a relatively rapid change in angle of attack through buffet onset and penetration with some variation in Mach number and altitude. The limits for the flight test conditions were either a maximum angle of attack of 18° or a maximum load factor of approximately 3g. The tunnel flow conditions were set to simulate the airplane average Mach number and dynamic pressure during the higher load, postbuffet portions of the maneuvers. However, it was not possible to change the model angle of attack at the rates experienced by the airplane (generally 1 to 5 deg/sec). The horizontal tails on both the airplane and model are used for pitch and roll control. However, on the model they are used as trim rather than maneuver devices and, hence, have a very slow deflection rate. Several studies have indicated that the maximum lift force attainable by a wing in unsteady motion increases with its pitch rate, that pitch rate tends to delay buffet onset and to increase the magnitude of the buffet loads. For high pitch rates such as might be encountered in helicopter or compressor blades the effect can be substantial, but for pitch rates comparable to those attainable by airplanes, even fighter types, these studies indicate the effect is generally less than a 10-percent increase in maximum lift coefficient for the Mach number range covered by the present studies. (See refs. 4 and 24, for example.) Evidence also suggests that the maximum buffet load at a given penetration into the buffet boundary tends to increase with time to some asymptotic value. The model, of course, can be subjected to the buffet flow for considerably longer periods than the maneuvering airplane, so that the pitch rate and time effects may tend to cancel.

The test technique used in the present buffet studies exhibited a deficiency in horizontal-tail load simulation that has since been minimized; that is, the deflection of the horizontal tails relative to the model angle of attack was not the same for the model and airplane. On the airplane, except for trimmed flight conditions, the instantaneous deflection angle of the horizontal tails relative to the instantaneous angle of attack for a particular dynamic pressure will vary, depending on the type of maneuver (rolling or straight pull-up), the suddenness of the tail deflection, and whether the deflection is to initiate or terminate the maneuver. On the model, however, the horizontal tails were used to statically trim the model to the required angle of attack. In addition, the model horizontal tails had to overcome a pitching moment that the full-scale tails did not have to contend with (the resisting moment of the cable-mount system) so that the effective tail power of the model was less than that of the airplane. A means has since been developed that allows horizontal-tail deflections independent of model angle of attack within certain limitations. A thin cable attached to the model forward of the effective pitch axis

extends vertically to a pitch-moment device located overhead outside the test section that is quite similar to the lift-balancing device described earlier. A load link is incorporated in the cable to allow determination of the pitching moment and lift that the device exerts on the model. With this system the tail buffet loads can be measured as a function of horizontal-tail deflection angle over a wide range of values for various discrete model angles of attack. Any effect of the cable on the model structural response can be minimized by attaching the cable near the fuselage vertical bending mode node line.

DISCUSSION OF RESULTS

Characteristics of Buffet Response

Power spectral density plots of the model structural response (bending moments and accelerations) were used to analyze the character of the buffet loads for the various flight conditions studied. Almost 500 plots were generated from which some conclusions can be made regarding the modal contributions to the total response. Many were repetitious and only samples or examples which serve to illustrate a point are presented in this report. Since the comparisons of model and airplane buffet spectra indicate that the model buffet characteristics were reasonably similar to those of the airplane, the power spectra of the various measurements made on the model were studied to determine the effect of wing sweep and Mach number on the modal contributions to the total response. Although there were some inconsistencies or anomalies, particularly in the horizontal-tail data, some general observations can be made, bearing in mind that because of the close proximity of frequencies of several of the natural vibration modes and because these frequencies may change some with flow velocity, it is sometimes difficult to ascribe a particular natural vibration mode to a particular "spike" on the power spectral density plot. In general, the modal composition of the total buffet response was dependent on the wing sweep angle, Mach number, and in some cases, depth of penetration into the buffet region.

Figure 8 shows some sample comparisons of model and airplane response spectra considered to be typical. The data are for a normal-force coefficient near that for maximum buffet.

Wing bending moment.- In figure 8(a) the right-wing bending moments of the model and airplane, normalized by the root-mean-square bending moments, are shown in terms of full-scale frequencies. The airplane data are from reference 12. The model and airplane wing bending-moment responses are seen to be almost the same and apparently consist solely of the wing first symmetrical bending mode. Measurements of wing normal shear force on the airplane indicated a slight contribution of the wing second bending mode to the total wing shear response. The model was not instrumented to measure this quantity. The peak response occurred at a frequency that correlated well with the wing

first symmetrical bending mode for all sweep angles and Mach numbers tested, both prior to buffet onset and during buffet. At very high values of normal-force coefficients, very slight amounts of energy were indicated at frequencies corresponding roughly to wing first torsion and/or horizontal-tail pitch.

Horizontal-tail bending moment.- Figure 8(b) compares the model horizontal-tail root bending-moment spectrum with unpublished airplane data for the left horizontal tail. Here the model response is primarily in the horizontal-tail first symmetrical bending mode with secondary response in the fuselage vertical bending mode. Unpublished airplane spectra indicate that the primary response varied between horizontal-tail bending and fuselage vertical bending depending on flight condition and whether the right or left tail was being considered. Some of the variance between airplane and model response may be due to the lack of simulation in some areas mentioned previously (slightly different pivot axis locations for the model and airplane and different tail deflection angles relative to the model and airplane angles of attack). At other Mach numbers and wing sweep angles the primary horizontal-tail bending-moment response also occurred at frequencies corresponding to the horizontal-tail symmetrical first bending frequency. Secondary responses (spectra peaks less than half the primary response peaks) apparently occurred in the horizontal-tail pitch, wing first torsion, wing first bending, and fuselage vertical bending modes with relative magnitudes dependent on Mach number, wing sweep angle, angle of attack, and horizontal-tail deflection angle. Since the tail deflection angle, angle of attack, and wing sweep angle could not be varied independently for these studies (see section "Testing Technique"), it was not possible to separate the effects of these parameters.

Center-of-gravity acceleration.- Figure 8(c) compares the acceleration spectrum of the model at the center of gravity with an unpublished airplane spectrum measured near the airplane nominal center of gravity for corresponding flow conditions. In this comparison the airplane spectrum reveals a large amount of energy, around 40 hertz, not indicated in the model spectrum. The source of this response is not known. It may be a local resonance of the structural member on which the accelerometer was mounted or, less likely, from the horizontal-tail antisymmetric torsion mode. Other available unpublished airplane acceleration spectra indicate that at other sweep angles this energy peak is much suppressed or not apparent. In these instances the primary airplane c.g. acceleration response was in the fuselage vertical bending mode as was the model response. The primary model response at all other wing sweeps and test Mach numbers was in the fuselage vertical bending mode. Secondary responses occurred in the horizontal-tail pitch mode with a limited amount of horizontal-tail fore-and-aft bending and wing first torsion modes. The relative magnitudes of the secondary responses were not as dependent on Mach number as was the case for pilot station accelerations.

Pilot station accelerations.- The model buffet studies included measurement of the acceleration response at the pilot station, as well as at the center of gravity. Figure 10, which compares the acceleration spectra of measurements made at the pilot station and center of gravity at the same time, illustrates that the character of buffet accelerations is dependent on the measurement location. At the pilot station the buffet acceleration response primarily consists of the wing symmetric second bending mode, whereas at the center of gravity, the primary response is in the fuselage vertical bending mode with a significant amount of energy in the horizontal-tail pitch mode. Such differences in the frequency content of the response are particularly significant in considerations of the acceleration environment to which sensitive avionics equipment may be subjected. It should be noted also that since the acceleration is proportional to the frequency squared, high frequency structural response can cause quite high rms accelerations even though the amplitude or stress level is low. The fallacy of specifying some limit magnitude of buffet acceleration at an arbitrary location, such as the center of gravity, without considering the primary frequencies involved in the response, their relationship to location on the structure, and the important resonant vibration characteristics of the devices is obvious.

Prior to buffet onset, or at low levels of buffet, energy appeared at several frequencies about equally, but as the buffet condition became more fully developed, one mode generally would become predominant. The primary response at all wing sweeps and Mach numbers was at a frequency corresponding to the wing second symmetrical bending mode. Secondary responses occurred at wing first bending, fuselage vertical bending, and some at the horizontal-tail fore-and-aft bending frequencies with the relative magnitudes depending on Mach number and wing sweep angle. At 26° sweep, the major secondary response was at the wing first symmetrical bending frequency with the amount of wing first bending energy relative to the primary response in wing second bending increasing with Mach number. At 50° and 72° sweep, the secondary response was at the fuselage vertical bending frequency instead of the wing first bending frequency as was the case for a wing sweep of 26°.

Figure 11 compares the magnitudes of the buffet rms accelerations measured on the model at the center of gravity and at the pilot station. The figure shows that the manner in which the buffet accelerations change with normal-force coefficient generally is the same at both locations and is characterized by a sharp increase in magnitude with increase in normal-force coefficient for all Mach numbers and wing sweep angles except at $M = 0.8$ and $M = 1.17$ at $\Lambda = 72^{\circ}$. For these conditions, the buffet accelerations at both locations remained at a relatively high constant level for all values of normal-force coefficient, a characteristic exhibited by the airplane at the higher Mach number at 72° sweep. The intensity of the buffet accelerations at the pilot station are seen to be generally less than at the center of gravity.

Comparisons of Scaled Model and Airplane Buffet Bending Moments and Accelerations

Power spectral density comparisons have shown that the model and airplane buffet response characteristics were reasonably similar. The root-mean-square levels of the airplane and buffet bending moments and accelerations predicted from model data normalized by airplane design values, are compared in figure 12. The degree of correlation ranges from good to bad, depending on wing sweep angle, Mach number, and type of measurement. Except as noted, buffet bending moments are shown for both the right and left wings on the model. Only the right airplane wing was instrumented. It is interesting to note that although buffet onset occurred on both model wings at the same value of normal-force coefficient, the right wing consistently exhibited a larger response than the left. In addition, the tare response of the right wing was consistently higher than for the left wing. (See fig. 9.) A possible explanation is that the right wing experienced an effective higher angle of attack than the left wing, either due to differential twist in the wings or due to differential flow angularity. During tests the model tended to roll to the left so that a less negative horizontal-tail deflection angle was consistently required for the left tail to keep the model in level flight.

Before assessing the comparisons shown in figure 12 it should be mentioned that for the flight data the Mach number decreases with increasing normal-force coefficient with most of the Mach number change occurring between the two largest values of normal-force coefficient. This decreasing Mach number during the maneuver may have an alleviating effect on the flight buffet response at the higher normal-force coefficients.

$\Lambda = 26^{\circ}$.- Figure 12(a) compares the wing and horizontal-tail buffet bending moments and the c.g. buffet accelerations for a wing sweep of 26° and a nominal Mach number of 0.52. The airplane Mach number varied from 0.53 at the lowest buffet normal-force coefficient to 0.49 at the highest whereas the model data were for $M = 0.52$. After buffet onset, the bending moments on both model wings increase rapidly with normal-force coefficient and compare favorably with the flight data. The apparent decrease in flight buffet bending moment indicated by the data point at the maximum C_N may be attributable to the decreasing Mach number or to normal scatter in the data. This amount of scatter would not be unusual for such flight measurements (ref. 4, for example) since the necessarily short data samples may not be long enough to exhibit completely stationary characteristics.

The airplane and model horizontal-tail buffet bending moments are seen to compare very well for the test condition of $\Lambda = 26^{\circ}$, $M = 0.52$. There was no consistency in the maximum bending moments occurring on a particular side, either on the model or the airplane.

The airplane c.g. buffet acceleration does not show the rapid increase in magnitude with normal-force coefficient exhibited by the model data. At $M = 0.76$ (fig. 12(b)), the decrease in airplane Mach number with increasing C_N is minimal (0.76 to 0.75) and for this case the model and airplane c.g. buffet accelerations both exhibit a rapid increase in intensity with increasing C_N and agree very well. The airplane and model wing and tail bending moments also are in good agreement.

Figure 12(c) compares model and airplane data for a nominal Mach number of 0.81 at a wing sweep of 26^o. The airplane Mach number varied from 0.83 to 0.81. All three measurements are seen to correlate very well.

$\Lambda = 50^o$.- At $M = 0.52$ and $\Lambda = 50^o$ (fig. 12(d)), the airplane and model wing buffet bending moment are reasonably comparable over the C_N range duplicated. Values of C_N greater than those indicated for the model were not attainable due to insufficient tail power as discussed earlier. The model right horizontal-tail bending moments are seen to increase much more rapidly than the model left tail moments or the airplane bending moments. The reader is reminded that the model horizontal-tail deflections normally were not the same as those of the airplane for equivalent normal-force coefficients. The model c.g. buffet accelerations are seen to increase almost linearly with C_N whereas the rate of increase for the airplane apparently decreases at the higher normal-force coefficients; this is also true at $M_M = 0.80$ (fig. 12(e)). The wing buffet bending moments predicted from model data tend to be slightly high as compared with those for the airplane. However, the horizontal-tail bending moments, perhaps fortuitously, are in good agreement over the test range of C_N. At a nominal $M = 0.90$ (fig. 12(f)), the predicted wing buffet bending moments for the model are seen to scatter about the almost linear airplane values. Little can be said of the horizontal-tail data other than that both the model and airplane data exhibit considerable scatter. The c.g. buffet accelerations predicted from model data follow the trend of increasing severity with increasing C_N, whereas the airplane measurements indicate little if any increase with C_N. One might question the almost instantaneous increase in airplane buffet acceleration from the onset value of (presumably) a little over 0.3 percent of the design load factor to a value in excess of 0.7 percent of design.

$\Lambda = 72^o$.- At $M_M = 0.52$ (fig. 12(g)), the airplane c.g. buffet accelerations are seen to remain constant with increasing C_N, whereas the predicted values tend to increase initially with increasing C_N to a maximum value slightly greater than the flight value and then to decrease slightly. The same trend is exhibited in the model wing and horizontal-tail bending moments. One may imagine that this trend is observable in the airplane wing buffet bending moments but no such trend is discernible in the airplane horizontal-tail data. No model data are presented for the right horizontal tail due to a failure of the strain gage.

At $M_M = 0.80$ $(M_A = 0.81$ to $0.76)$ (fig. 12(h)), the model wing buffet bending moments again indicate increasing severity with increasing C_N to an apparent maximum value and are generally larger than the flight buffet levels at the higher levels of C_N. (Once again the airplane Mach number decreased substantially at the higher normal-force values.) Both model and airplane horizontal-tail data show considerable scatter with the airplane bending moments generally greater than those predicted by the model. The trends of the model and airplane c.g. buffet acceleration are comparable although the model accelerations are higher than the airplane accelerations. Also, this is the first instance where the model c.g. acceleration variation with C_N was not the same as the wing bending-moment variation.

The limited model data at $M_A = 1.17$ (fig. 12(i)) does not compare well with the airplane data. Model buffet onset occurred at a considerably lower value of C_N than the airplane buffet onset, and lack of model tail power accounted for the small overlap of the model and airplane data. At comparable values of C_N, the model and airplane wing buffet bending moments are in good agreement (no model data were obtained for the left wing due to strain-gage failure). Both the model and airplane exhibited very low wing buffet response (less than 1/4 percent of airplane design). The horizontal-tail bending moments predicted from model data are about the same magnitude as the airplane data, and the model c.g. buffet accelerations are relatively high compared with those on the airplane.

It is felt that the model data at the higher sweep angles and higher Mach numbers could be improved by using a smooth skin type instead of the segmented type construction. The small discontinuities caused by the edges of the wing segments are more nearly parallel to the airflow at the lower sweep angles but are presented more normal to the flow as the wing sweep increases. At the higher Mach numbers they provide sources for the generation of small shocks which can disturb the boundary layer and may cause premature separation.

CONCLUDING REMARKS

A wind-tunnel technique which employs complete dynamically scaled aeroelastic models for predicting airplane buffet loads has been evaluated. The buffet bending moments and accelerations measured on a flutter model of a fighter airplane are compared with those measured on the airplane in an independent flight buffet research study. Some pertinent observations follow.

Although the model used in the study was a flutter model and was not specifically designed for buffet load studies, analysis of the model vibration characteristics and the modal character of the model and airplane structural response to buffet flow indicated

that the model adequately simulated the airplane structure. Even with this type of elaborate cable-mounted flutter model, practical considerations call for some compromises such as lack of simulation of pitch rates and Reynolds number. To improve boundary-layer simulation on the model, a smooth skin construction technique instead of the segmented approach is recommended.

Potential improvements in technique were identified, such as providing supplementary means of changing angle of attack so that horizontal-tail deflections could be made independent of model angle of attack.

Power spectral density analyses of the model response to buffet flow showed that the indicated modal composition of the total measured response was dependent on the type and location of the measurement, wing sweep angle, Mach number, and, in some cases, the depth of penetration into the buffet region.

The normal-force coefficients at which buffet onset occurred on the airplane were generally very close to those predicted by the model except for the 72° wing sweep configuration. At this sweep angle, buffeting began on the model at significantly lower normal-force coefficients than indicated for the airplane.

The full-scale buffet bending moments on the wing and horizontal tails and the c.g. buffet accelerations predicted from the model data agreed well with airplane values at all Mach numbers at a wing sweep angle of 26°. At a wing sweep of 50°, the agreement was reasonably good at all Mach numbers tested for the wing bending moments, but the correlation of the model and airplane c.g. accelerations and horizontal-tail bending moments was not as good at the higher Mach numbers. At 72° sweep, both the airplane and model data exhibited a large degree of randomness at extremely low levels of buffet response which made evaluation of the correlation difficult. However, the airplane and model loads were of the same general magnitude.

Langley Research Center,
National Aeronautics and Space Administration,
Hampton, Va., December 18, 1972.

REFERENCES

1. Liepmann, H. W.: On the Application of Statistical Concepts to the Buffeting Problem. J. Aeronaut. Sci., vol. 19, no. 12, Dec. 1952, pp. 793-800, 822.

2. Rainey, A. Gerald; and Byrdsong, Thomas A. (With Appendix A by Don D. Davis, Jr.): An Examination of Methods of Buffeting Analysis Based on Experiments With Wings of Varying Stiffness. NASA TN D-3, 1959.

3. Pearcey, H. H.: A Method for the Prediction of the Onset of Buffeting and Other Separation Effects From Wind Tunnel Tests on Rigid Models. AGARD Rep. 223, Oct. 1958.

4. Huston, Wilber B.; and Skopinski, T. H.: Measurement and Analysis of Wing and Tail Buffeting Loads on a Fighter Airplane. NACA Rep. 1219, 1955. (Supersedes NACA TN 3080.)

5. Huston, Wilber B.; Rainey, A. Gerald; and Baker, Thomas F.: A Study of the Correlation Between Flight and Wind-Tunnel Buffeting Loads. NACA RM L55E16b, 1955.

6. Seal, Diana M.: A Survey of Buffeting Loads. C.P. No. 584, Brit. A.R.C., 1962.

7. Husk, D. I.: The Influence of the Major Design Parameters Upon the Buffet Boundaries of a Wing. Presented at 14th Meeting of Structures and Materials Panel of AGARD (Paris), July 1962.

8. Rigby, Robert N.; and Cornette, Elden S.: Wind-Tunnel Investigation of Tail Buffet at Subsonic and Transonic Speeds Employing a Dynamic Elastic Aircraft Model. NASA TN D-1362, 1962.

9. Mabey, D. G.: Measurements of Wing Buffeting on a Scimitar Model. C.P. No. 954, Brit. A.R.C., 1967.

10. Mabey, D. G.: An Hypothesis for the Prediction of Flight Penetration of Wing Buffeting From Dynamic Tests on Wind Tunnel Models. C.P. No. 1171, Brit. A.R.C., 1971.

11. Hollingsworth, E. G.; and Cohen, M.: Comparison of Wind Tunnel and Flight Test Techniques for Determining Transonic Buffet Characteristics on the McDonnell Douglas F-4 Airplane. J. Aircraft, vol. 8, no. 10, Oct. 1971, pp. 757-763.

12. Friend, Edward L.; and Monaghan, Richard C.: Flight Measurements of Buffet Characteristics of the F-111A Variable-Sweep Airplane. NASA TM X-1876, 1969.

13. Mechtly, E. A.: The International System of Units – Physical Constants and Conversion Factors (Revised). NASA SP-7012, 1969.

14. Speaker, W. V.; and Ailman, C. M.: Spectra and Space-Time Correlations of the Fluctuating Pressures at a Wall Beneath a Supersonic Turbulent Boundary Layer Perturbed by Steps and Shock Waves. NASA CR-486, 1966.

15. McCanless, George F., Jr.: Additional Correction of 4% Saturn V Protuberance Test Data. Tech. Rep. HSM-R1-71 (Contract NAS 8-30517), Space Div., Chrysler Corp., Jan. 21, 1971. (Available as NASA CR-103064.)

16. Mabey, D. G.: Flow Unsteadiness and Model Vibration in Wind Tunnels at Subsonic and Transonic Speeds. C.P. No. 1155, Brit. A.R.C., 1971.

17. Bisplinghoff, Raymond L.; Ashley, Holt; and Halfman, Robert L.: Aeroelasticity. Addison-Wesley Pub. Co., Inc., c.1955.

18. Reed, Wilmer H., III; and Abbott, Frank T., Jr.: A New "Free-Flight" Mount System for High-Speed Wind-Tunnel Flutter Models. Proceedings of Symposium on Aeroelastic & Dynamic Modeling Technology, RTD-TDR-63-4197, Pt. I, U.S. Air Force, Mar. 1964, pp. 169-206.

19. Rice, S. O.: Mathematical Analysis of Random Noise. Bell System Tech. J.
Pts. I and II, vol. XXIII, no. 3, July 1944, pp. 282-332.
Pts. III and IV, vol. XXIV, no. 1, Jan. 1945, pp. 46-156.

20. Doggett, Robert V., Jr.; and Hanson, Perry W.: An Aeroelastic Model Approach for the Prediction of Buffet Bending Loads on Launch Vehicles. NASA TN D-2022, 1963.

21. Rainey, A. Gerald: Measurement of Aerodynamic Forces for Various Mean Angles of Attack on an Airfoil Oscillating in Pitch and on Two Finite-Span Wings Oscillating in Bending With Emphasis on Damping in the Stall. NACA Rep. 1305, 1957. (Supersedes NACA TN 3643.)

22. Hanson, Perry W.; and Doggett, Robert V., Jr.: Aerodynamic Damping and Buffet Response of an Aeroelastic Model of the Saturn I Block II Launch Vehicle. NASA TN D-2713, 1965.

23. Davis, Don D., Jr.; and Wornom, Dewey E.: Buffet Tests of an Attack-Airplane Model With Emphasis on Analysis of Data From Wind-Tunnel Tests. NACA RM L57H13, 1958.

24. Conner, Fox; Willey, Craig; and Twomey, William: A Flight and Wind Tunnel Investigation of the Effect of Angle-of-Attack Rate on Maximum Lift Coefficient. NASA CR-321, 1965.

TABLE I.- FLUTTER MODEL NOMINAL SCALE FACTORS

Parameter	Symbol	Airplane-to-model ratio
Reduced stiffness	$k_r = (b\omega/V)_r$	*1.195
Length	b_r	8.0
Mach number	M_r	1.0
Velocity	V_r	*2.232
Frequency	ω_r	1/3
Airstream density	ρ_r	*1.457
Dynamic pressure	q_r	*7.258
Stiffness	$(EI)_r$, $(GJ)_r$	42 450
Mass	m_r	745.9
Mass moment of inertia	I_r	47 736
Mass density	$\left(\frac{m}{b^3\rho}\right)_r$	*1.0

*For the buffet test conditions, these values vary slightly. (See section in text entitled "Scaling Considerations" and table III.)

TABLE II.- SAMPLE COMPARISONS OF STRUCTURAL DAMPING AND SCALED MODEL FREQUENCIES WITH AIRPLANE VALUES

Symmetrical mode	C_s/C_{cr}		f, Hz	
	Model	Airplane	Model	Airplane
$\Lambda = 26^o$				
Wing first bending	0.008	0.009	5.23	5.15
Wing second bending	.012	.010	15.3	15.3
Wing torsion	.010	.020	25.3	25.4
Fuselage vertical bending	.008	.009	7.4	7.6
Horizontal-tail bending	.014	.010	13.3	13.3
Horizontal-tail pitch	.010	----	32.4	32.7
$\Lambda = 50^o$				
Wing first bending	0.007	0.009	4.9	5.1
Wing second bending	.008	.007	15.1	16.7
Wing torsion	----	.018	25.7	26.4
Fuselage vertical bending	.005	.009	7.4	7.5
Horizontal-tail bending	.016	.020	13.4	13.3
Horizontal-tail pitch	.010	----	31.7	32.7
$\Lambda = 72^o$				
Wing first bending	0.012	0.010	4.9	5.1
Wing second bending	.007	.022	15.2	16.2
Wing torsion	----	.020	27.7	26.6
Fuselage vertical bending	----	.009	7.4	7.5
Horizontal-tail bending	----	.018	13.0	13.3
Horizontal-tail pitch	----	----	31.0	32.7

TABLE III.- SUMMARY OF SCALE RATIOS AND MODEL AERODYNAMIC DAMPING COEFFICIENTS USED TO SCALE MODEL BUFFET DATA TO AIRPLANE VALUES

Λ, deg	M	ρ_r	V_r	q_r	$k_r^{1/2}$	K_D	Mode (a)	$\left(\frac{C_a}{C_{cr}}\right)_M$	$\left(\frac{C_T}{C_{cr}}\right)_r^{-1/2}$	K_σ	K_a
26	0.52	1.582	2.130	7.18	1.119	0.859	W1B	0.0878	1.065	4380	----
							FVB	.1676	1.072	----	0.740
							HTB	.1670	1.085	4455	----
	0.76	1.945	1.923	7.20	1.117	0.962	W1B	0.0878	1.013	4400	----
							FVB	.1676	1.015	----	0.740
							HTB	.1670	1.030	4470	----
	0.81	1.962	1.970	7.62	1.164	0.995	W1B	0.0942	0.998	4535	----
							FVB	.1803	.956	----	0.727
							HTB	.1795	1.013	4600	----
50	0.52	1.618	2.121	7.29	1.121	0.883	W1B	0.1282	1.052	4410	----
							FVB	.2272	1.052	----	0.738
							HTB	.2463	1.052	4410	----
	0.80	2.075	1.952	7.90	1.168	1.043	W1B	0.1017	0.972	4590	----
							FVB	.1802	.970	----	0.768
							HTB	.1955	.970	4580	----
	0.90	2.120	1.928	7.86	1.172	1.052	W1B	0.0885	0.968	4235	----
							FVB	.1568	.965	----	0.762
							HTB	.1700	.990	4330	----
72	0.52	1.618	2.103	7.17	1.125	0.876	W1B	0.1270	1.070	4420	----
							FVB	.2403	1.051	----	0.732
							HTB	.2138	1.057	4365	----
	0.80	2.185	1.952	8.34	1.169	1.097	W1B	0.0964	0.968	4835	----
							FVB	.1823	.949	----	0.795
							HTB	.1622	.954	4765	----
	1.17	1.704	2.050	7.22	1.140	0.900	W1B	0.1403	1.058	4455	----
							FVB	.2652	1.044	----	0.737
							HTB	.2360	1.046	4400	----

[a] W1B, wing first bending; FVB, fuselage vertical bending; HTB, horizontal-tail bending.

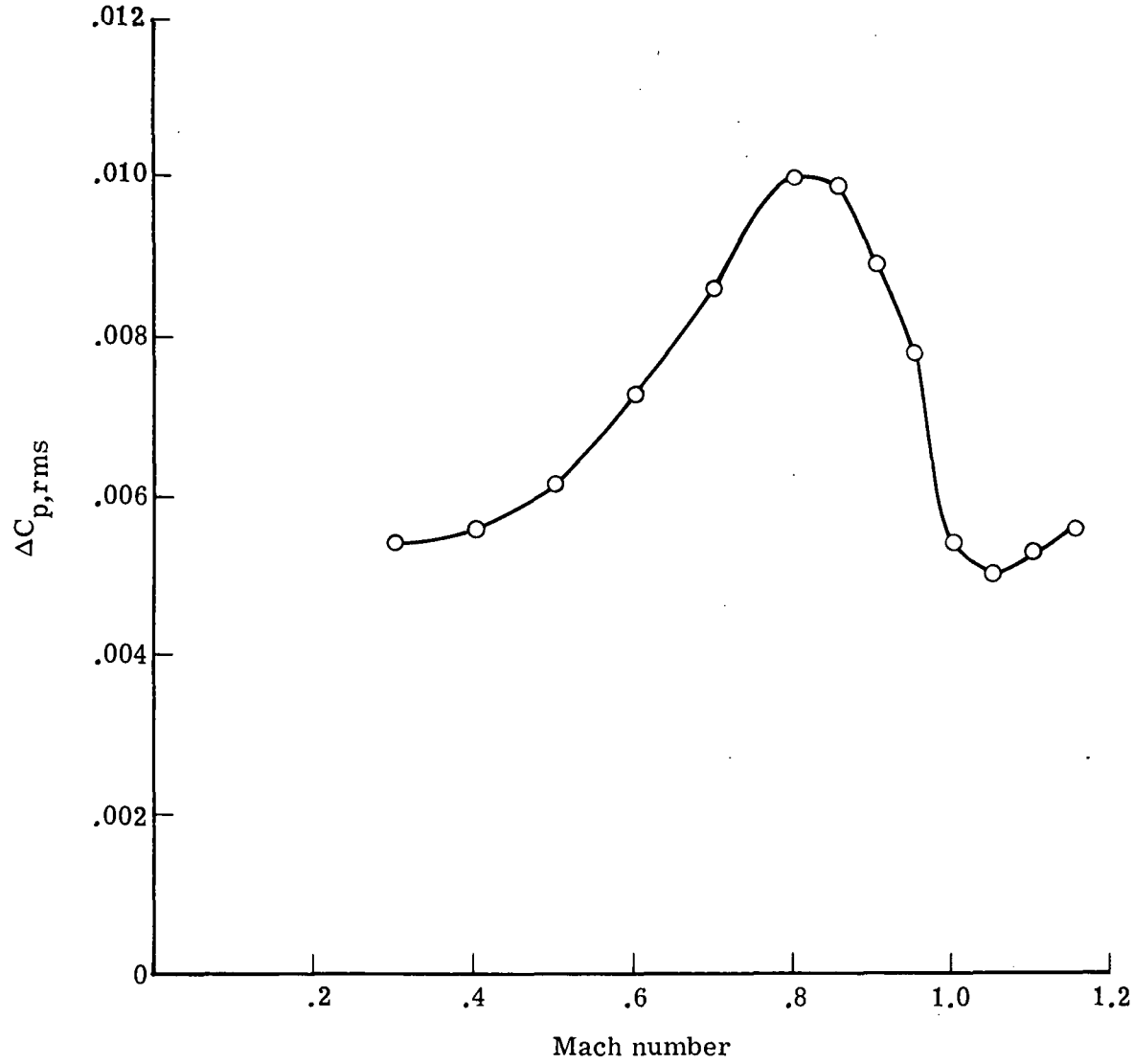

(a) Variation of sidewall fluctuating pressure with Mach number for maximum dynamic-pressure operation.

Figure 1.- Fluctuating pressure characteristics of Langley transonic dynamics tunnel.

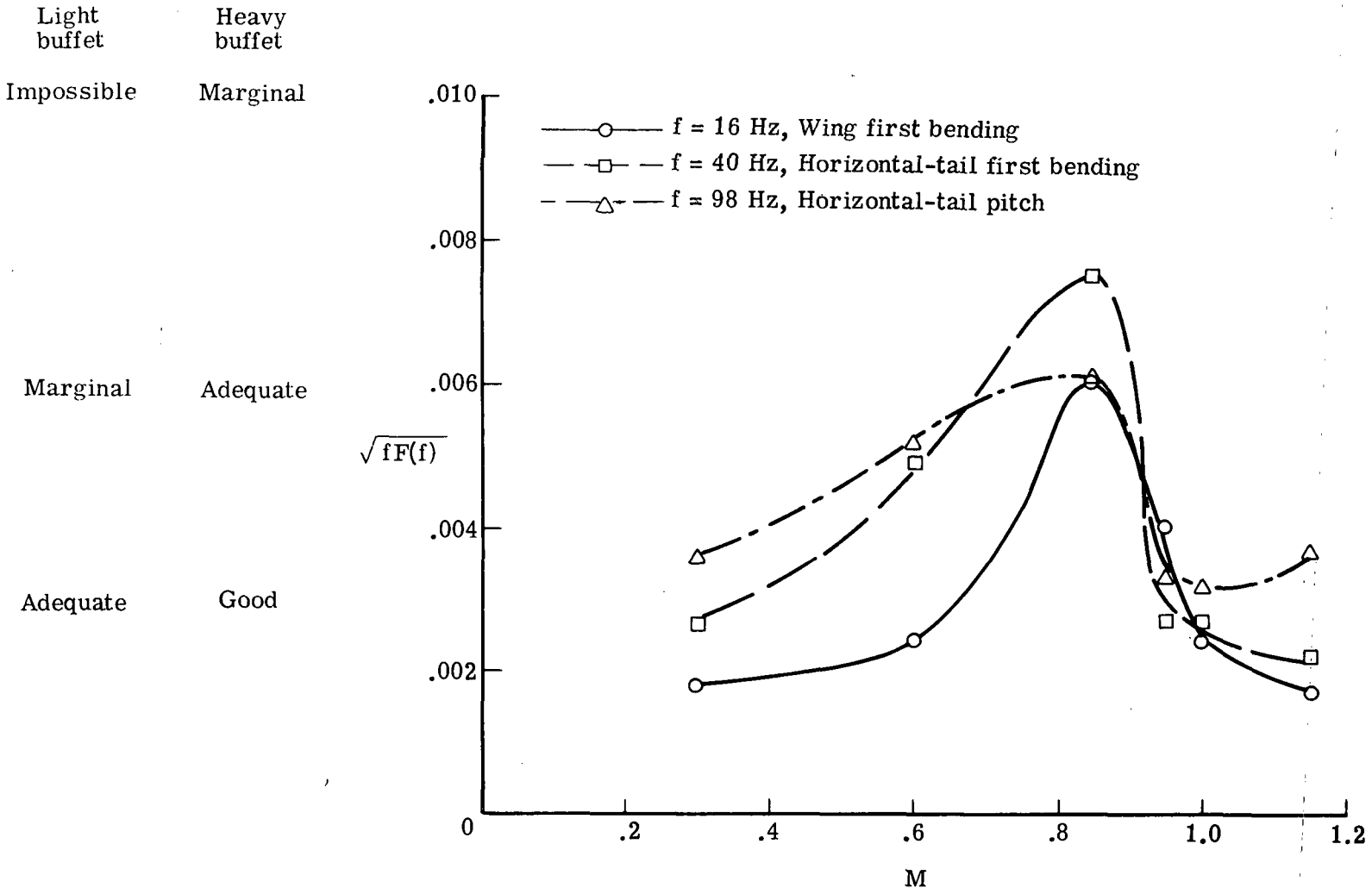

(b) Variation of sidewall fluctuating pressure power spectrum at pertinent discrete frequencies as a function of Mach number in Langley transonic dynamics tunnel. Test medium, Freon-12; empty tunnel.

Figure 1.- Concluded.

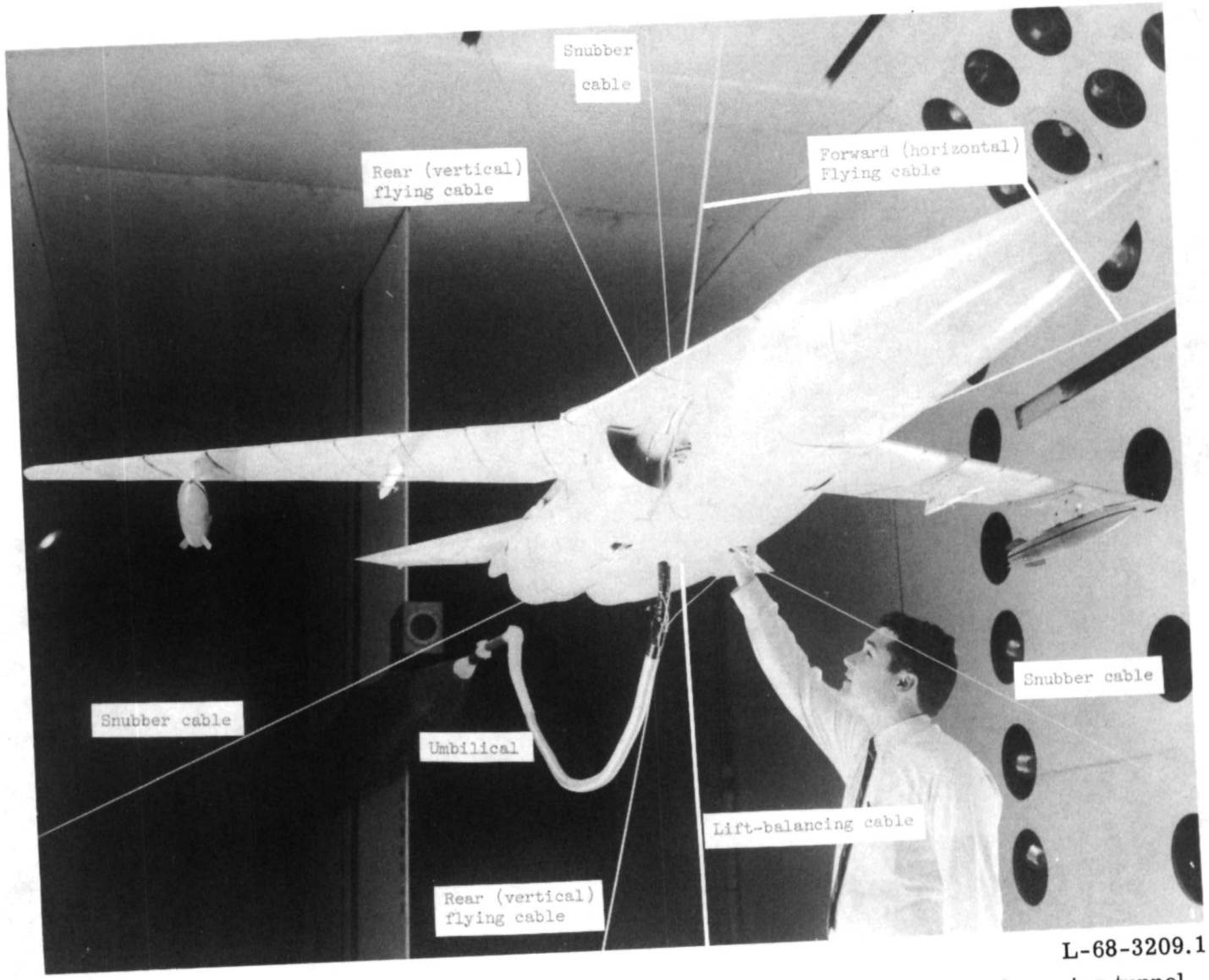

Figure 2.- Photograph of 1/8-scale flutter model mounted in Langley transonic dynamics tunnel.

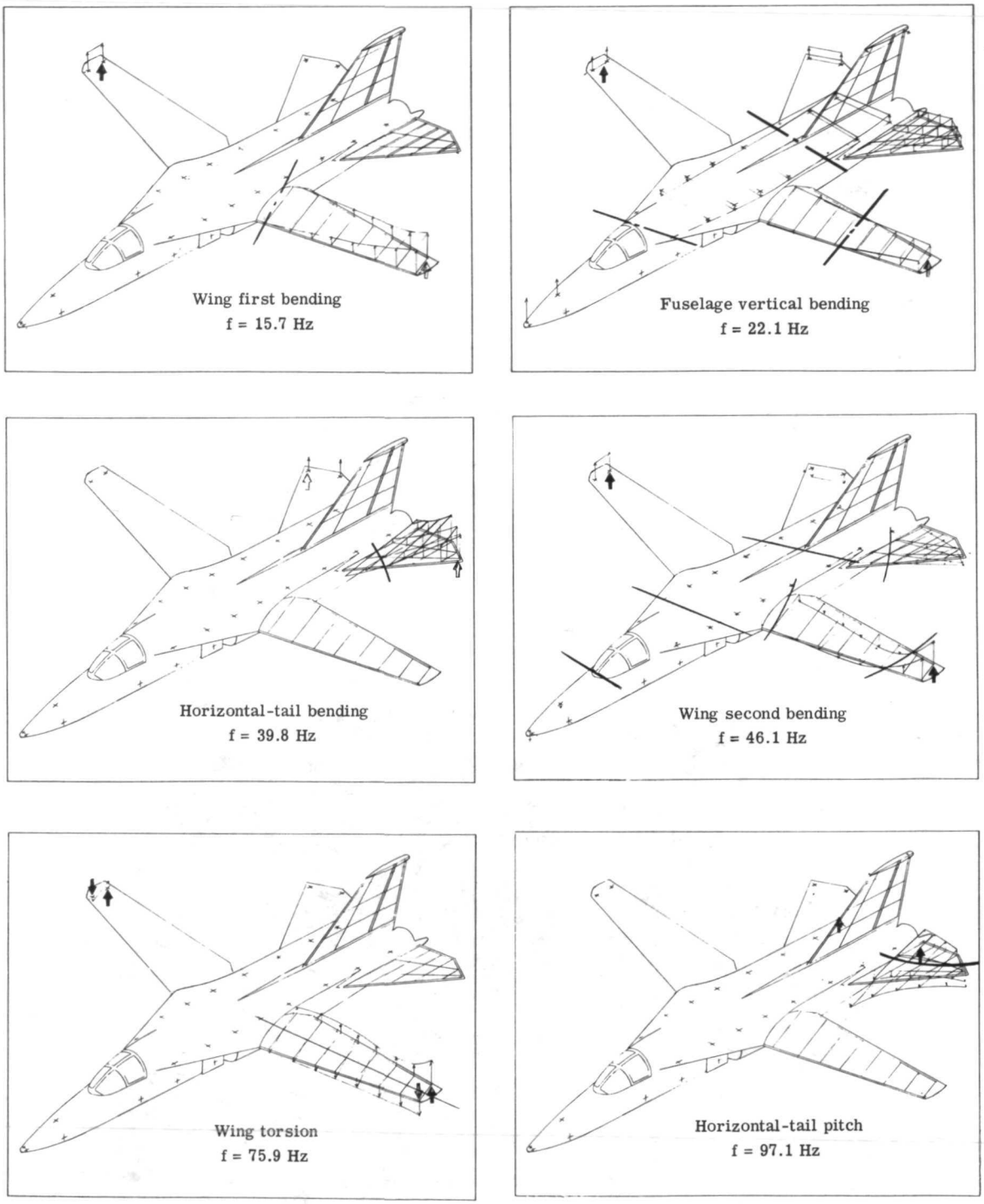

(a) $\Lambda = 26^{o}$.

Figure 3.- Model natural vibration mode shapes and frequencies. Heavy arrows indicate shaker locations.

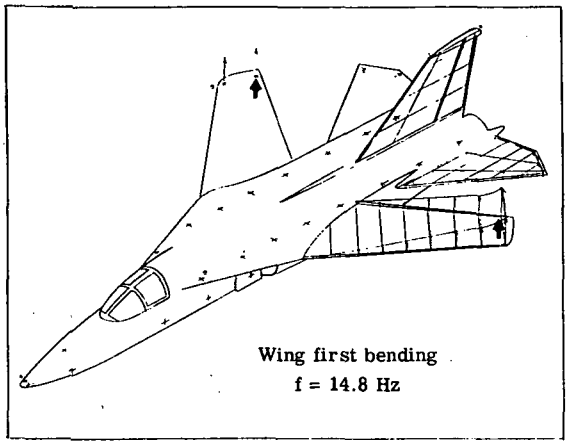

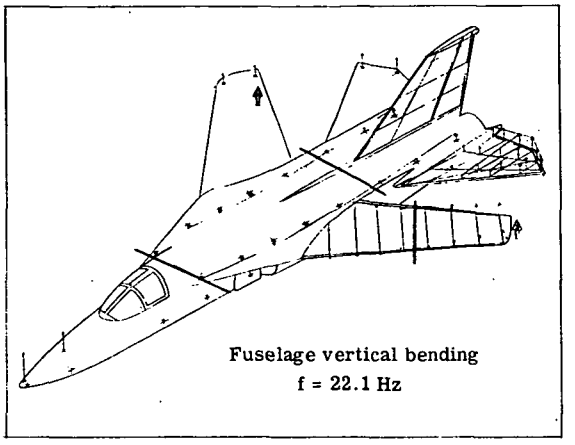

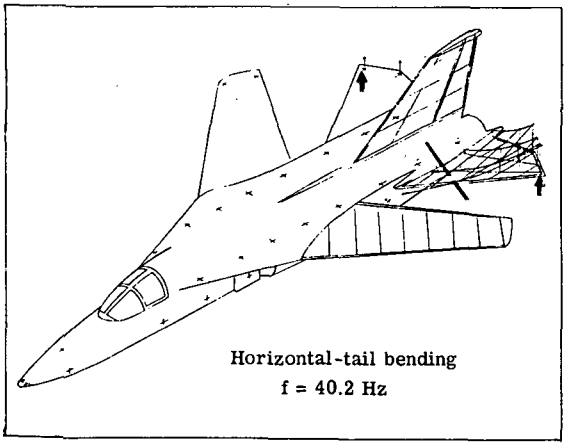

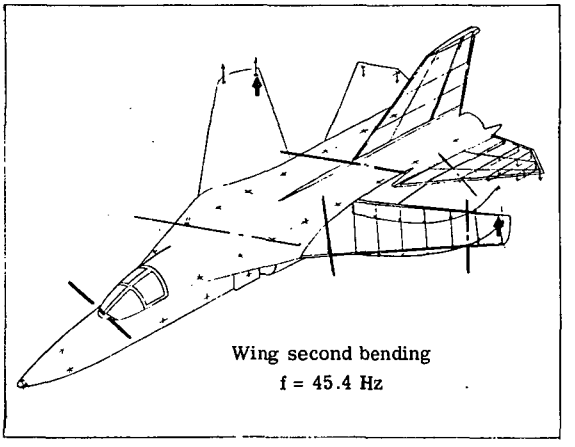

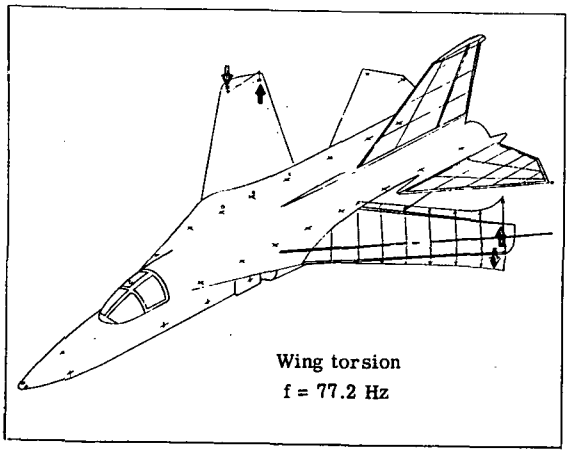

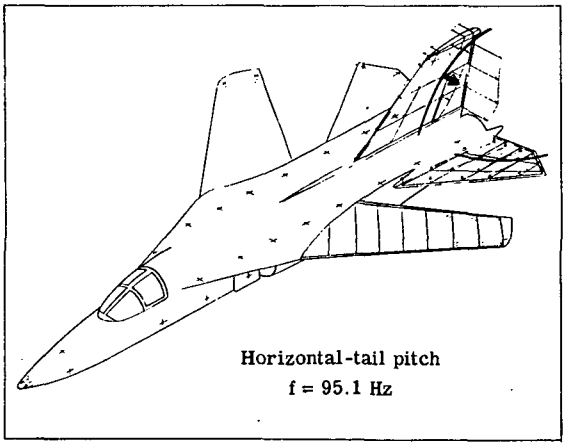

(b) $\Lambda = 50^{o}$.

Figure 3.- Continued.

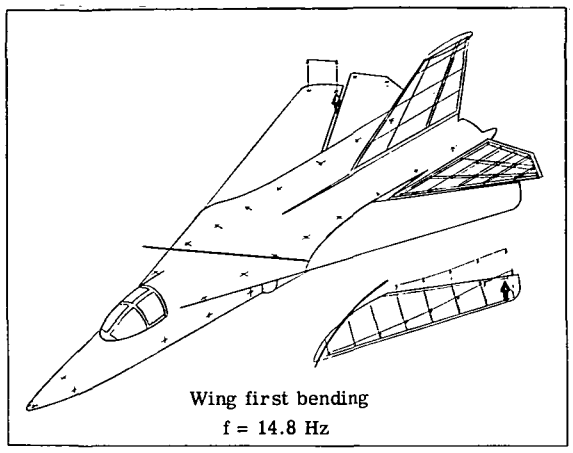

Wing first bending
f = 14.8 Hz

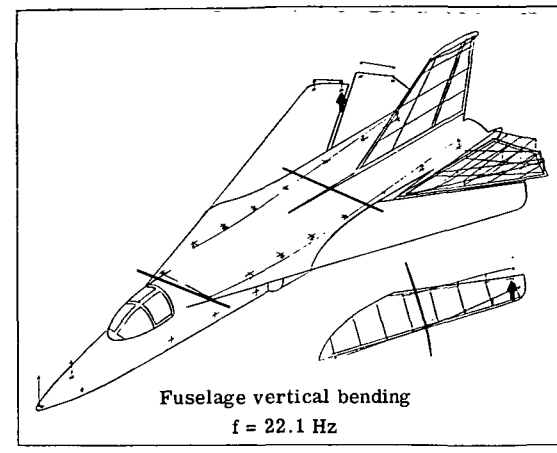

Fuselage vertical bending
f = 22.1 Hz

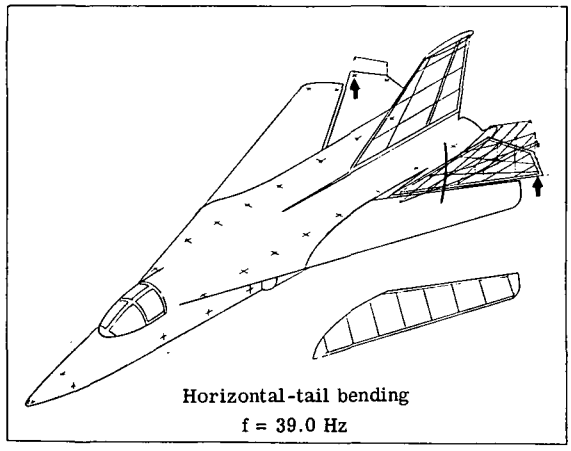

Horizontal-tail bending
f = 39.0 Hz

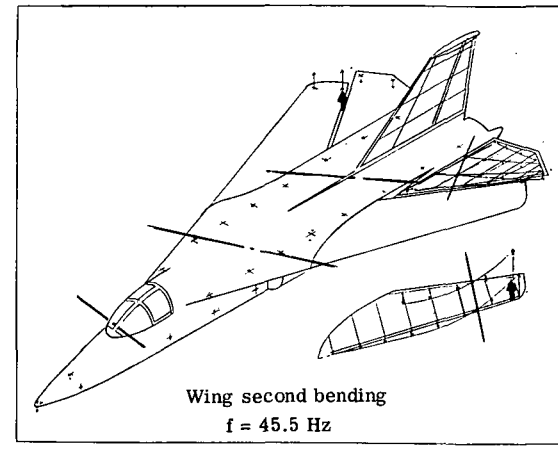

Wing second bending
f = 45.5 Hz

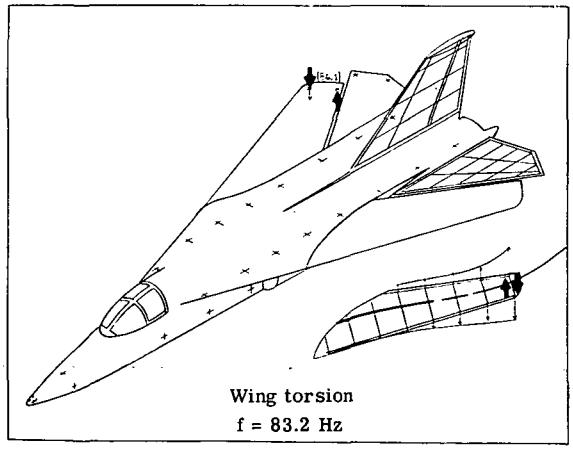

Wing torsion
f = 83.2 Hz

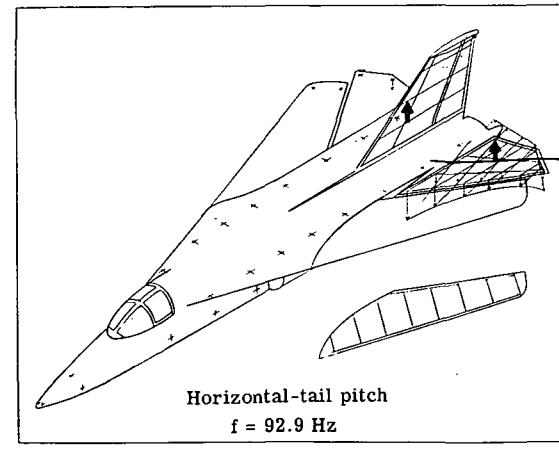

Horizontal-tail pitch
f = 92.9 Hz

(c) $\Lambda = 72^{\circ}$.

Figure 3.- Concluded.

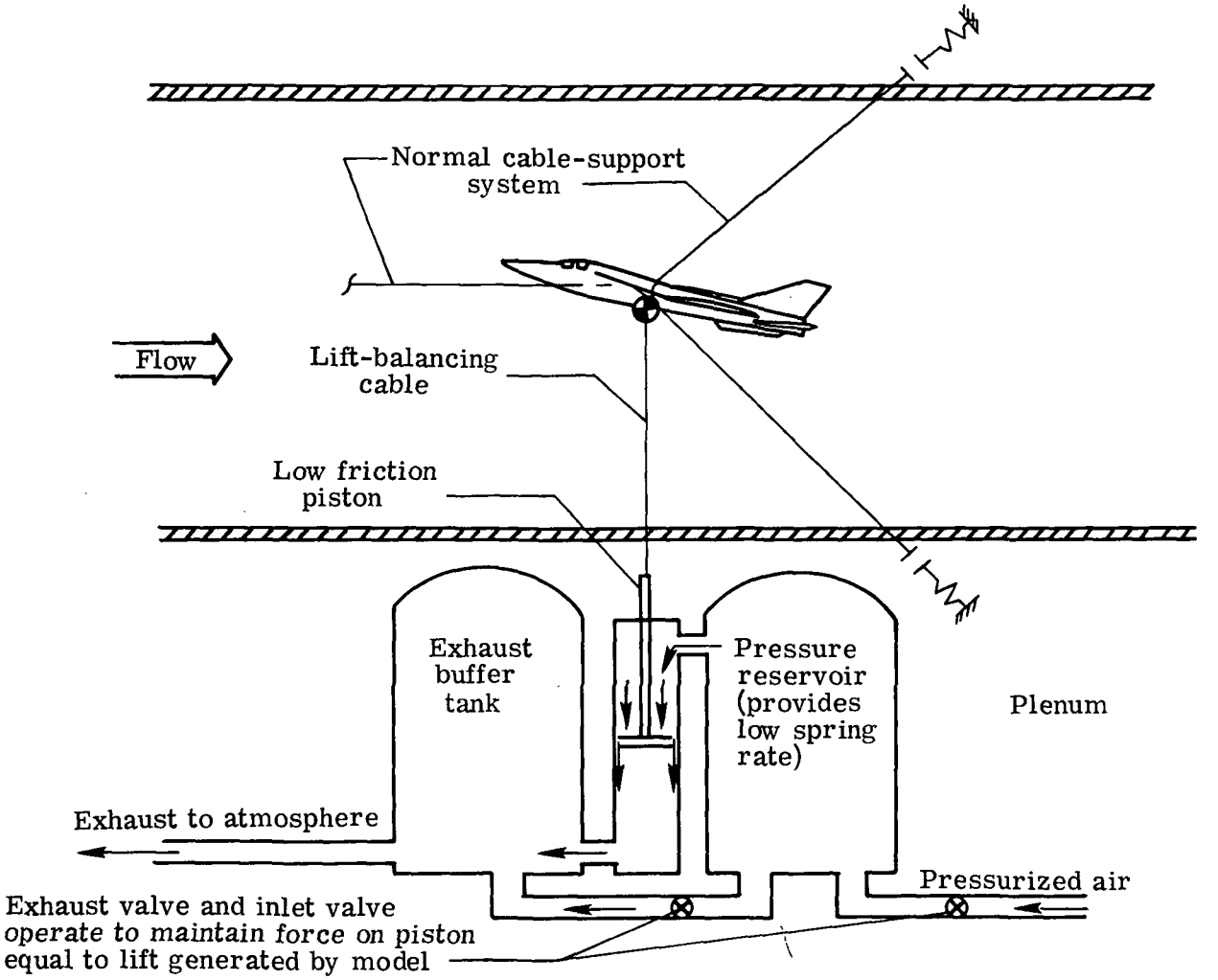

Figure 4.- Lift-balancing device for testing models at high lift coefficient.

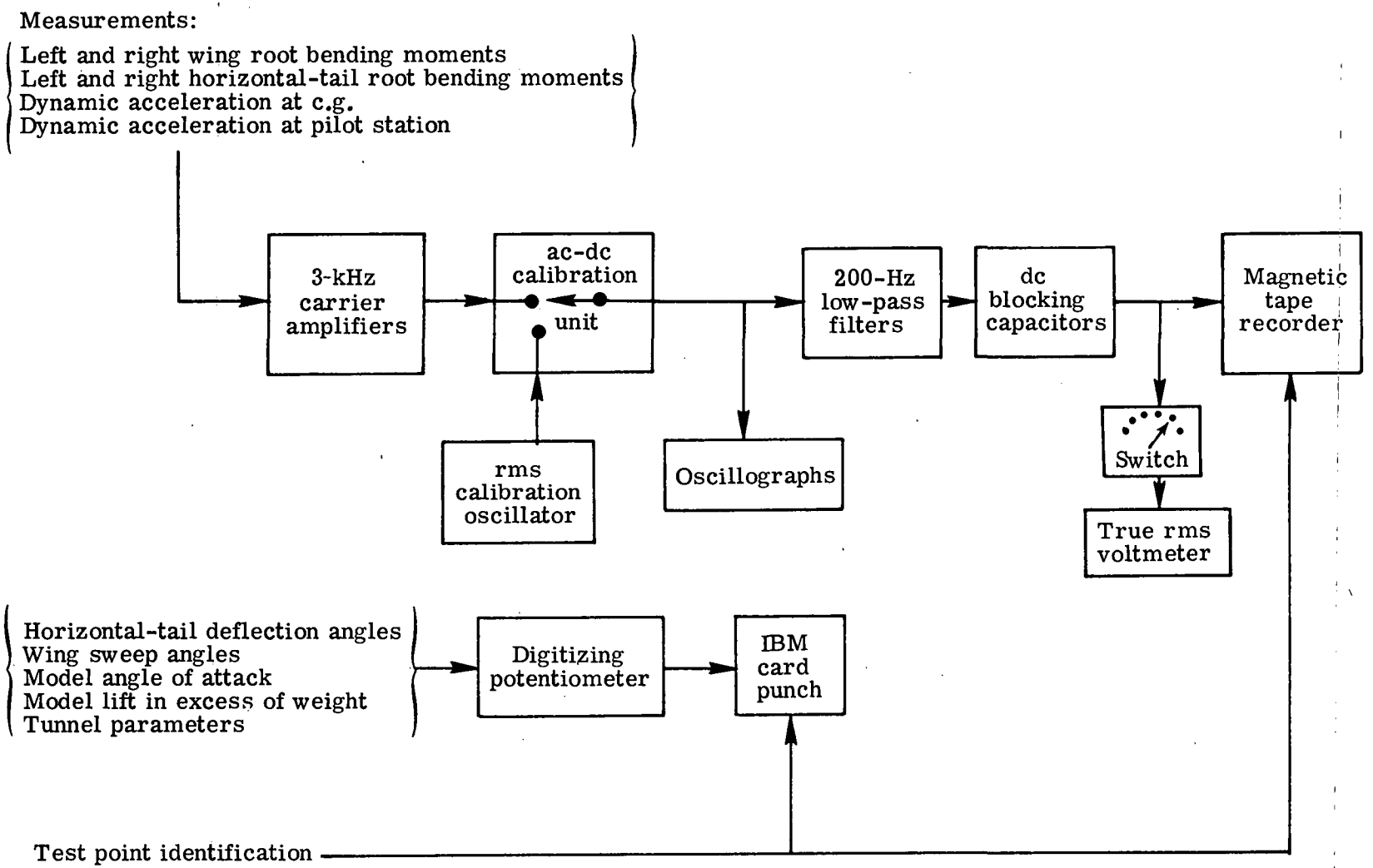

Figure 5.- Schematic diagram of data recording instrumentation.

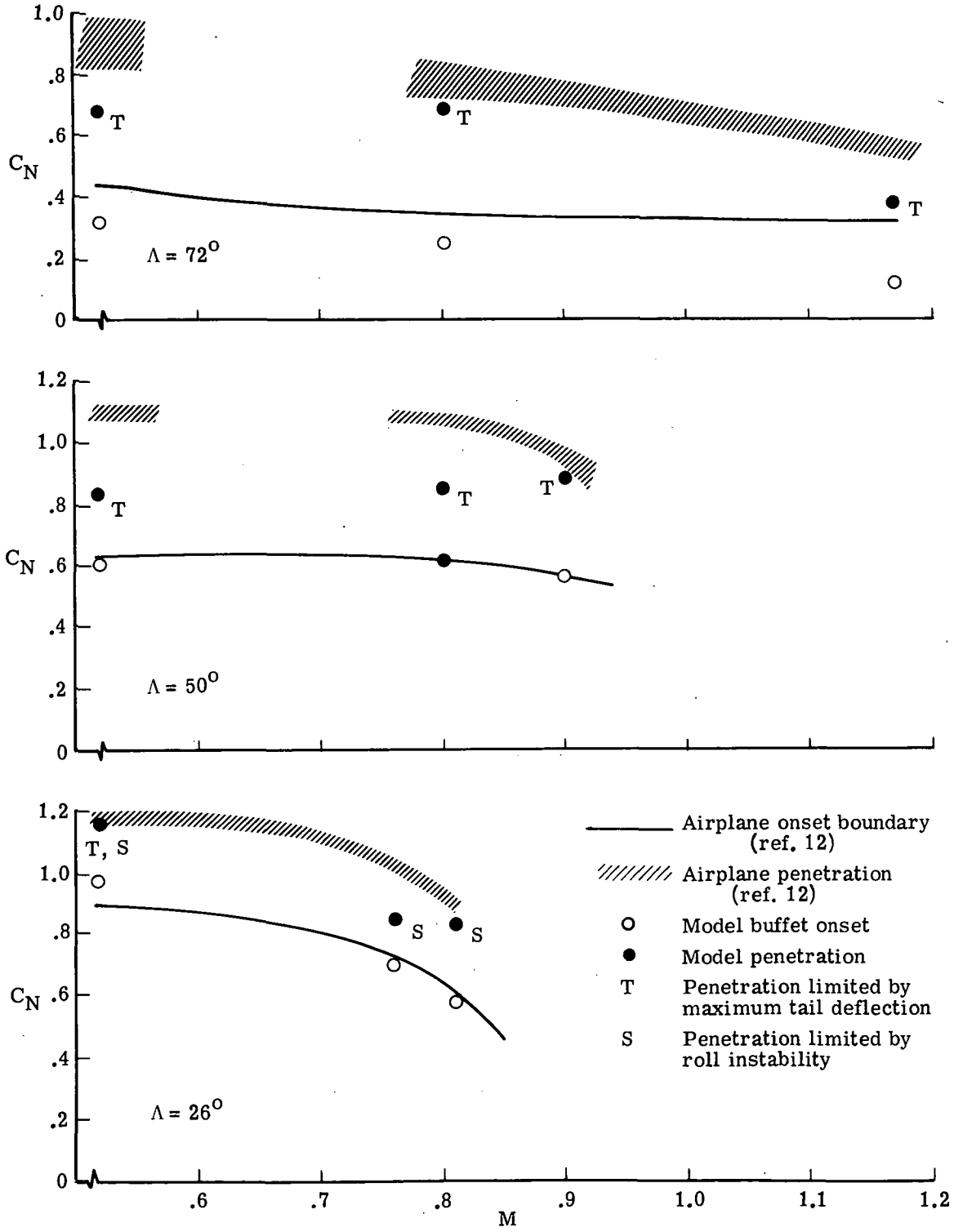

Figure 6.- Comparison of model and airplane buffet onset and boundary penetration.

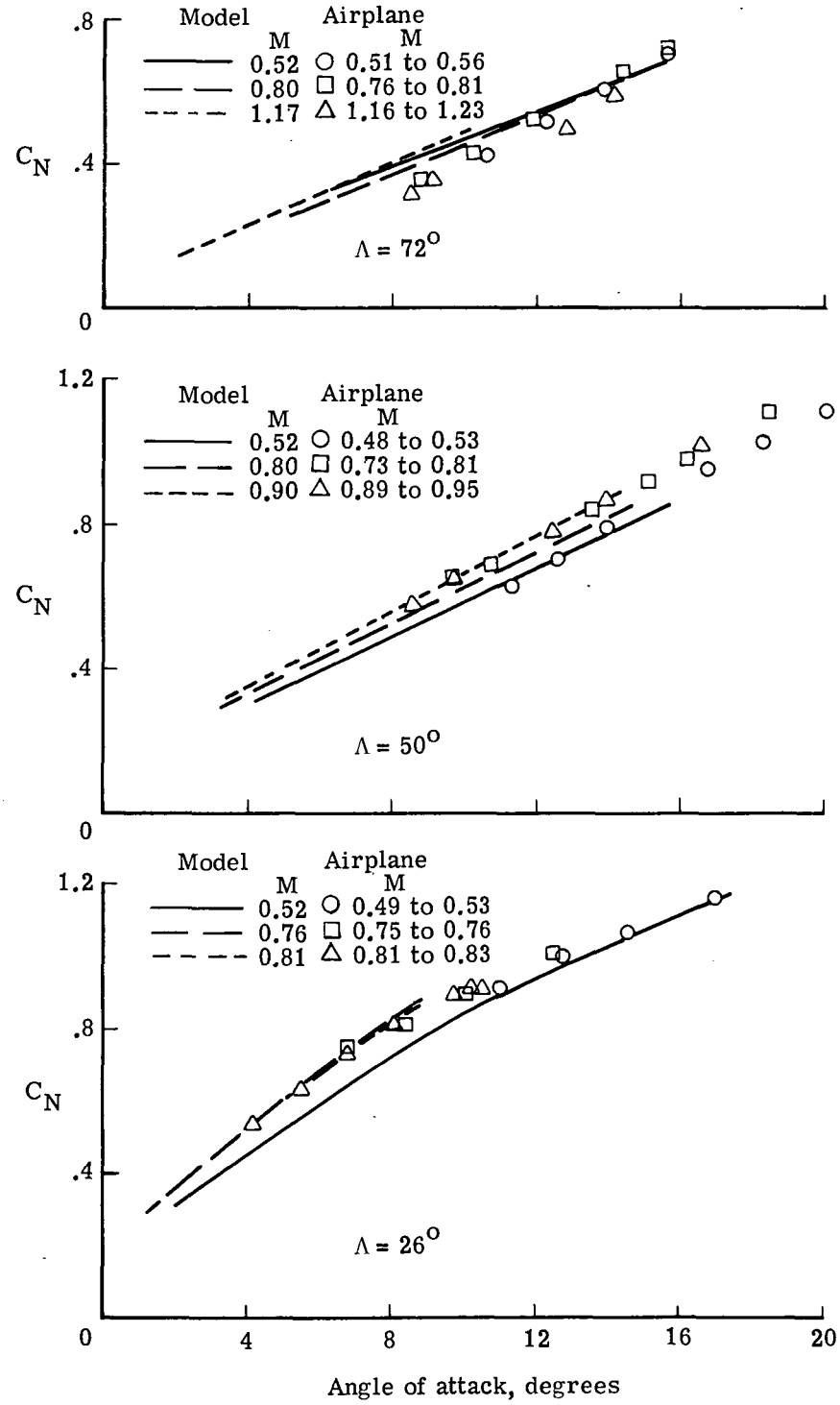

Figure 7.- Comparison of model and airplane C_N variation with angle of attack.

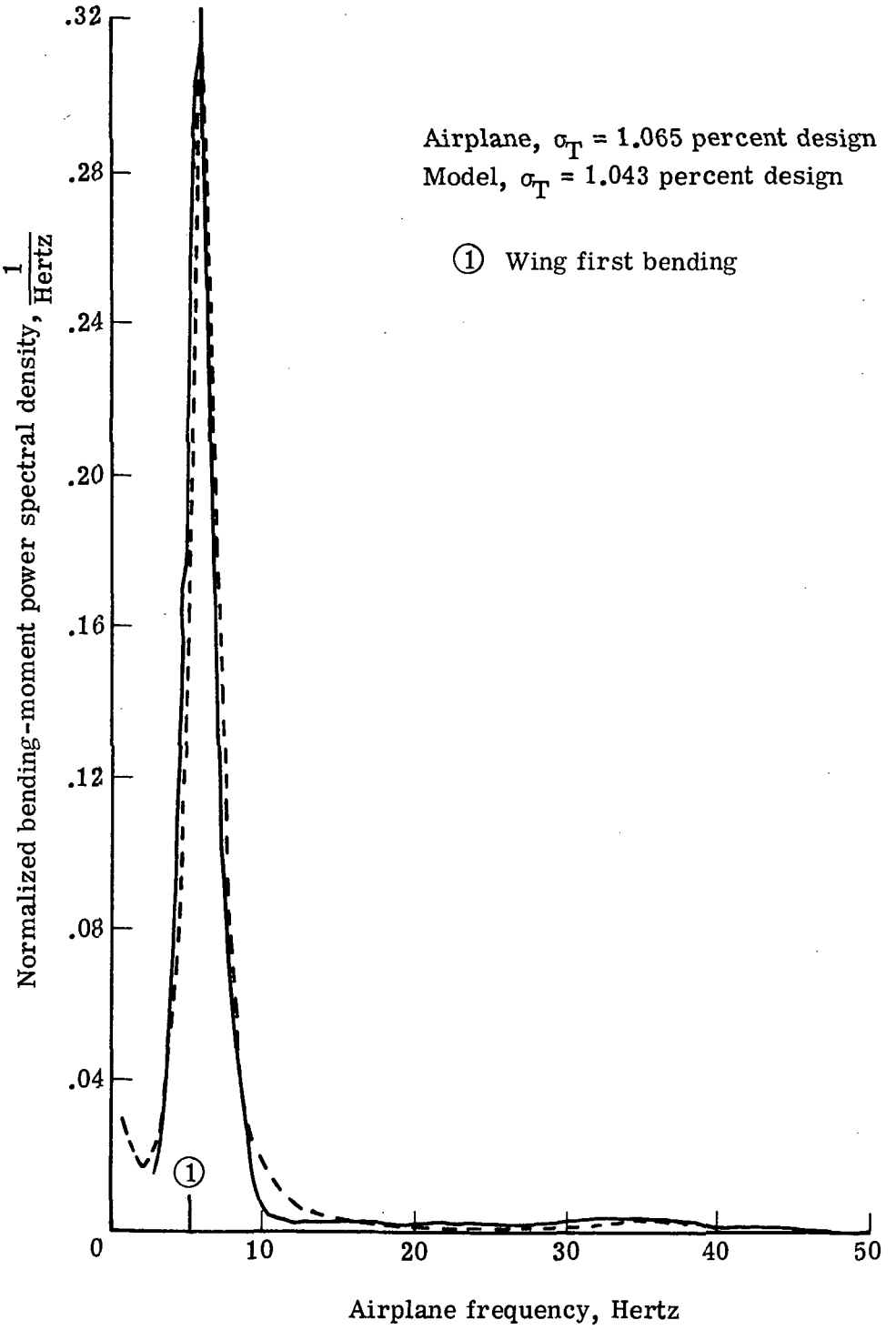

(a) Right wing bending moment.

Figure 8.- Sample comparisons of model and airplane response spectra. $\Lambda = 26^{o}$; M = 0.81; spectra normalized on rms level.

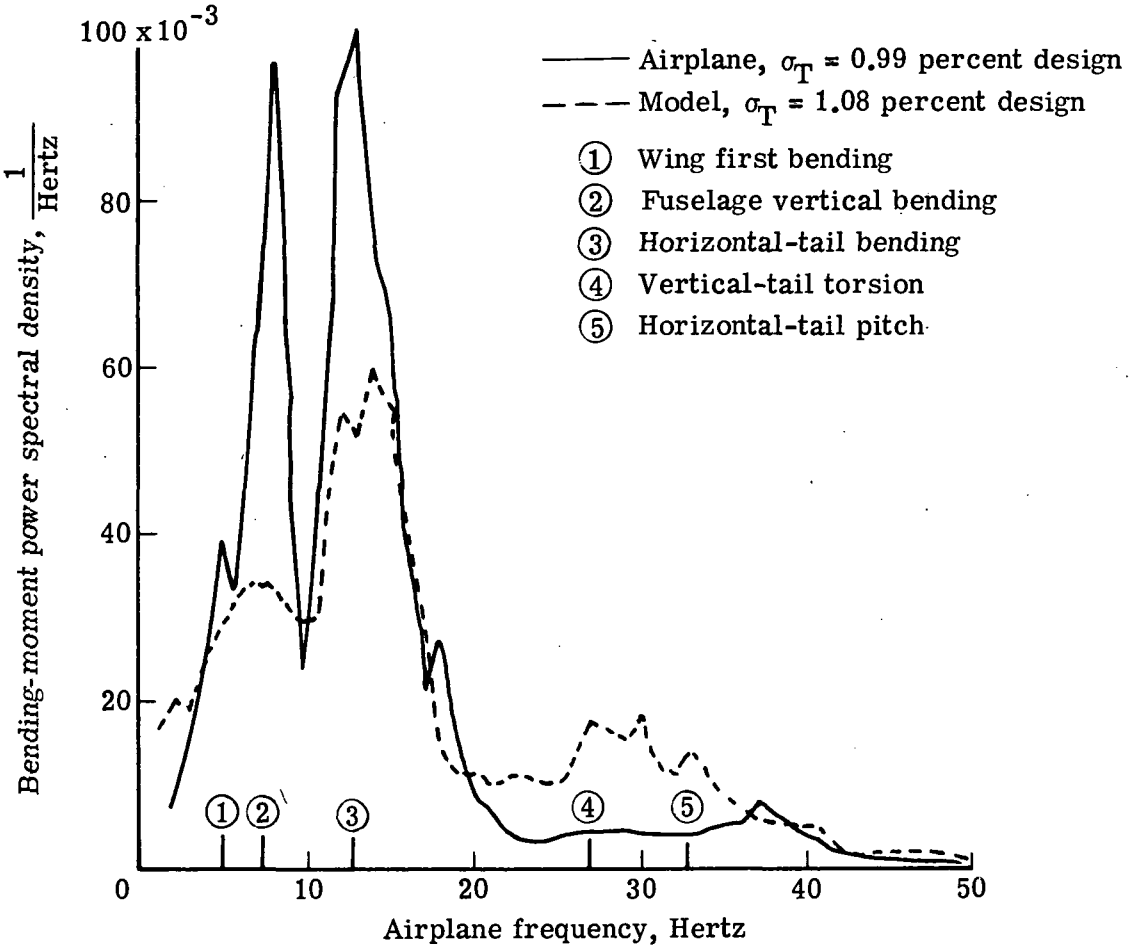

(b) Left horizontal-tail bending moment.

Figure 8.- Continued.

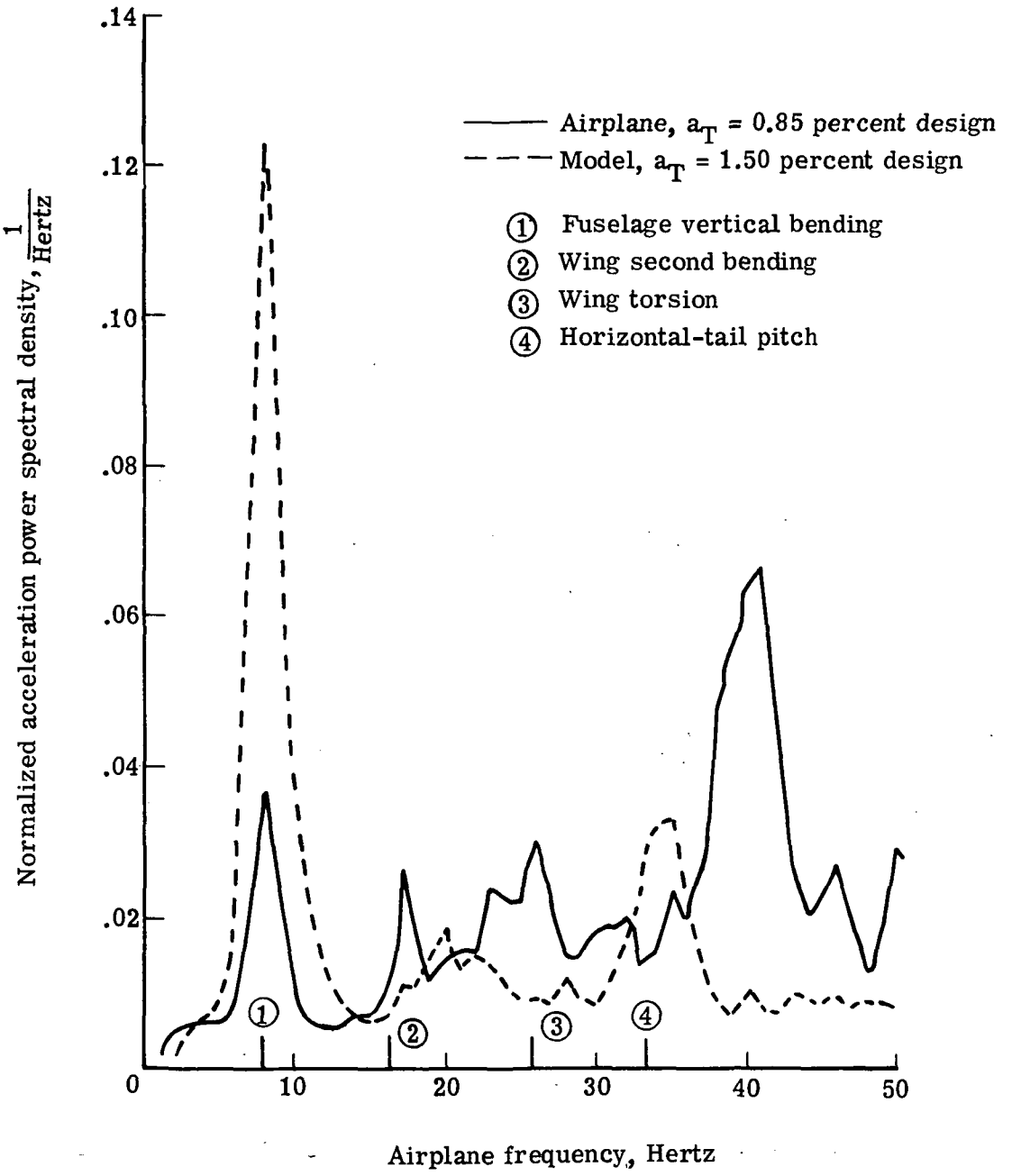

(c) Acceleration at center of gravity.

Figure 8.- Concluded.

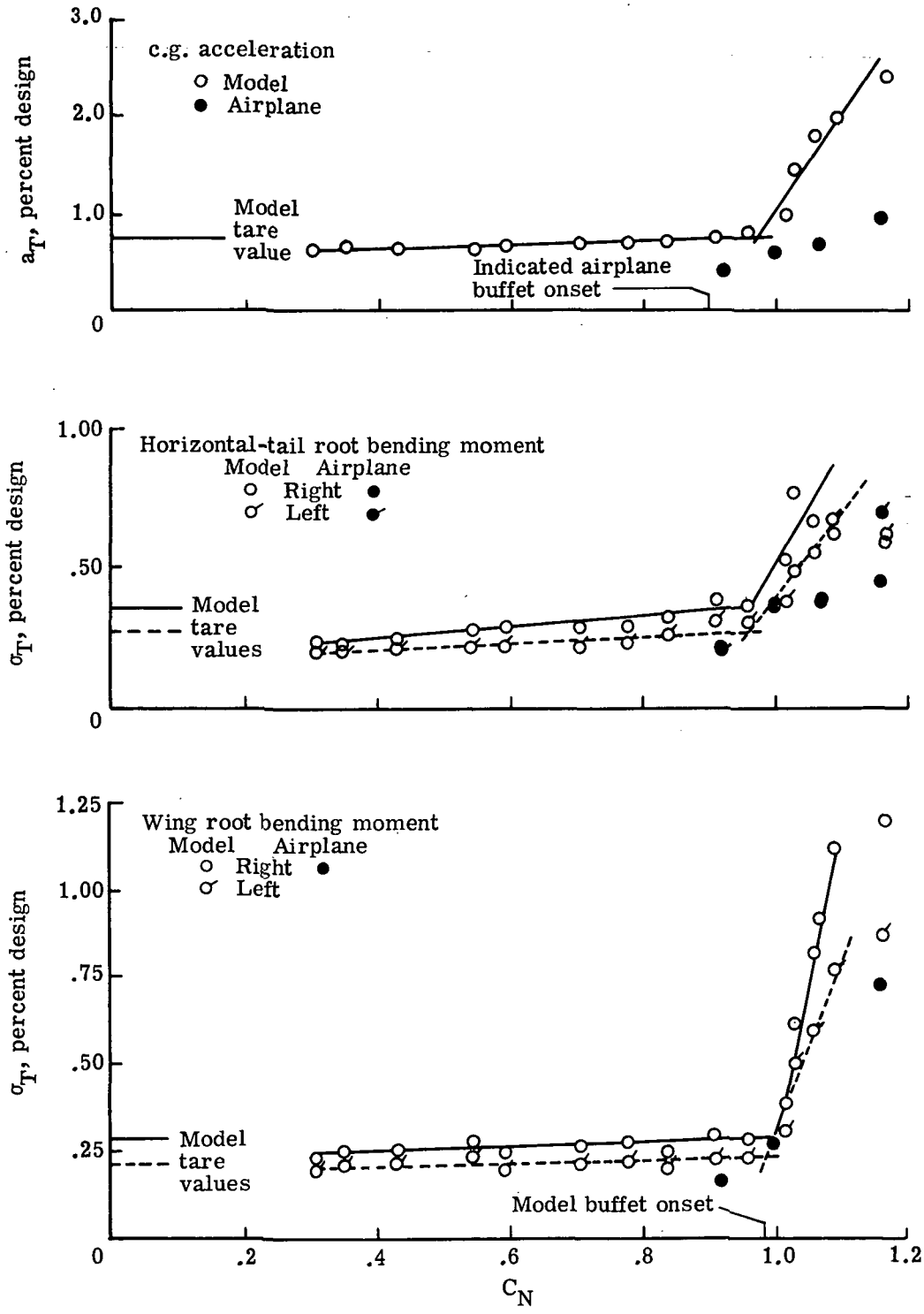

(a) Total response at $\Lambda = 26^{o}$. $M_M = 0.52$; $M_A = 0.53$ to 0.49.

Figure 9.- Model and airplane total response illustrating method of determining levels of buffet response and onset values.

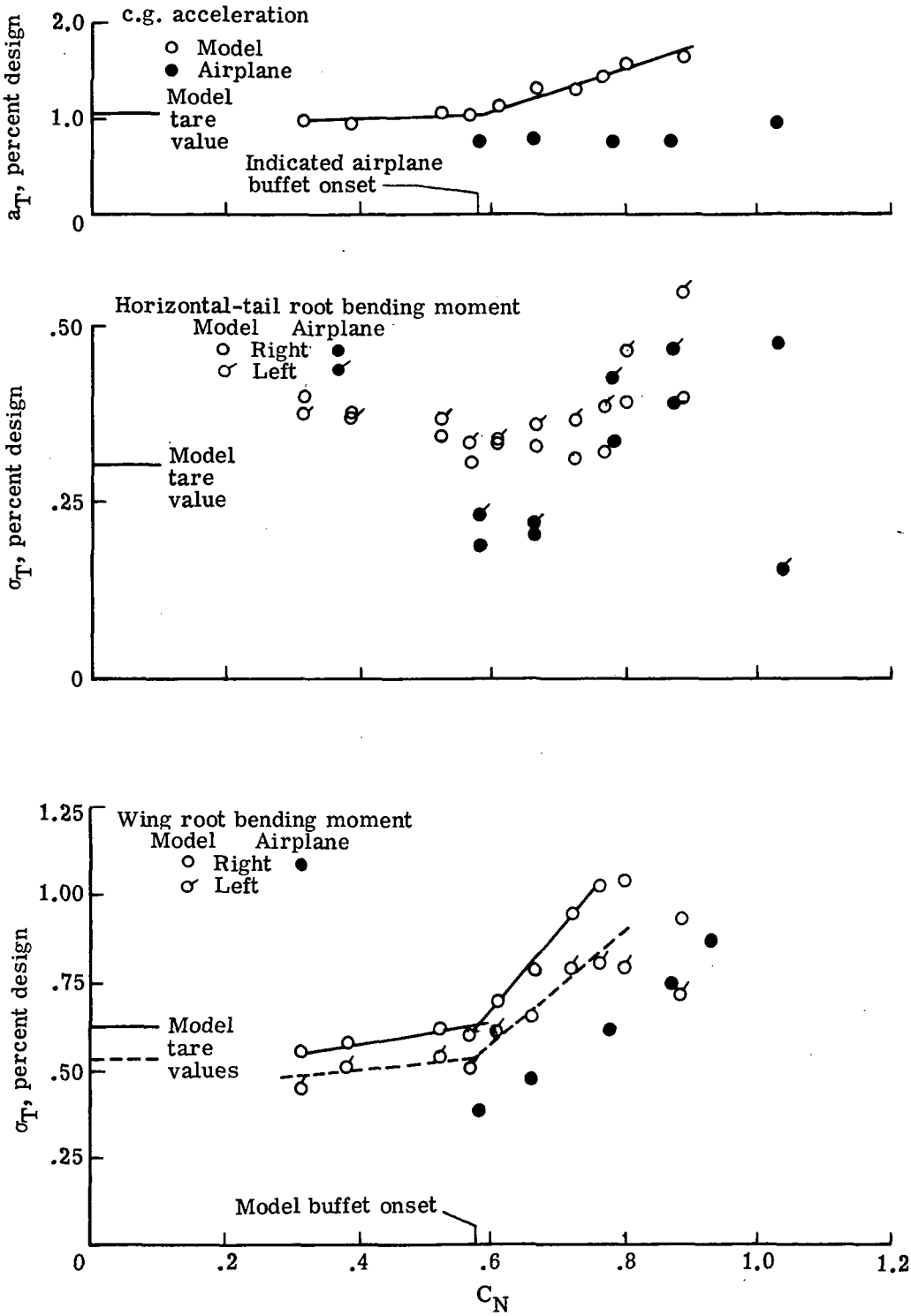

(b) Total response at $\Lambda = 50^{o}$. $M_M = 0.90$; $M_A = 0.95$ to 0.89.

Figure 9.- Concluded.

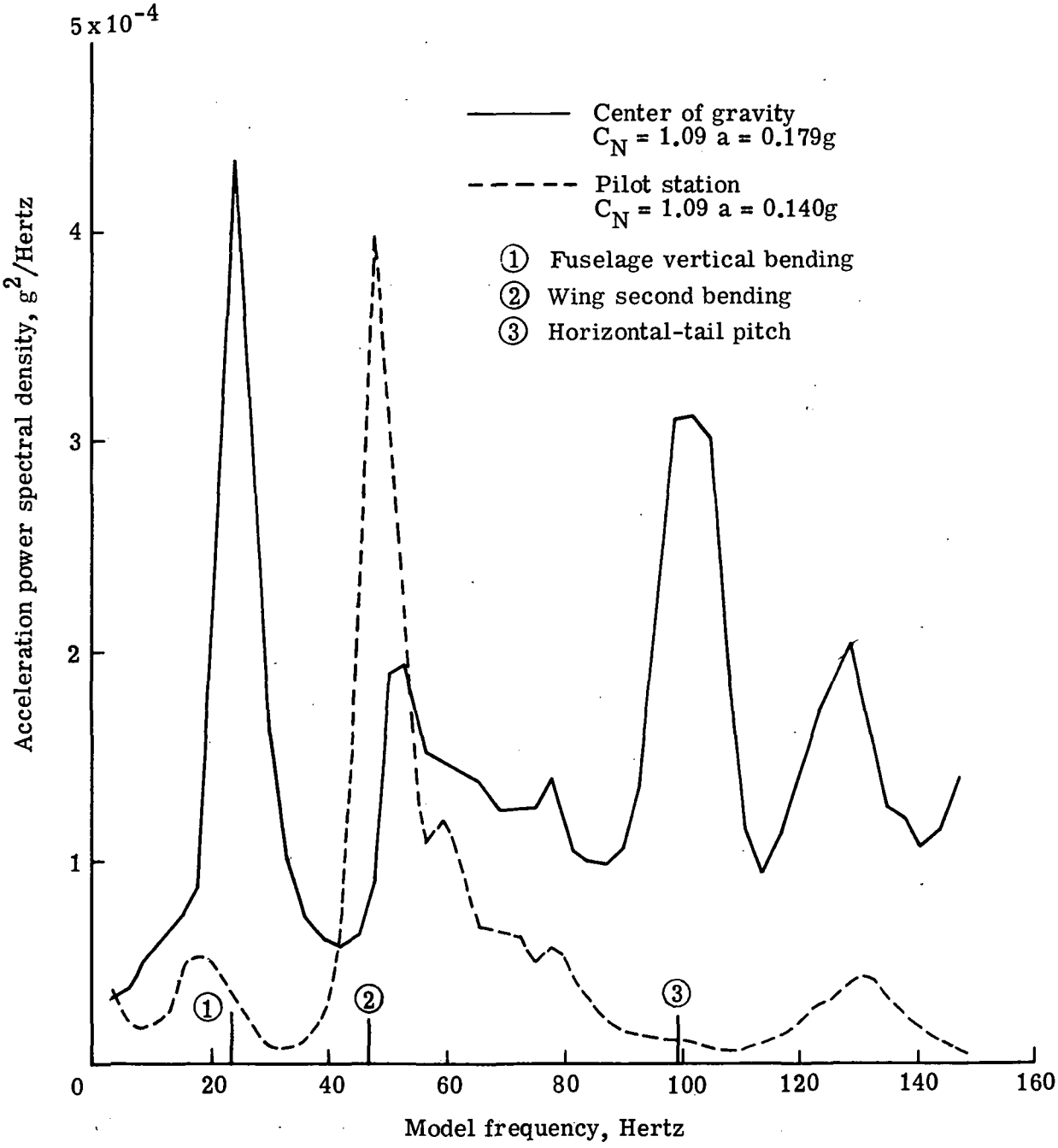

Figure 10.- Comparison of buffet acceleration spectra at center of gravity and pilot station. $\Lambda = 26^{o}$; $M = 0.52$.

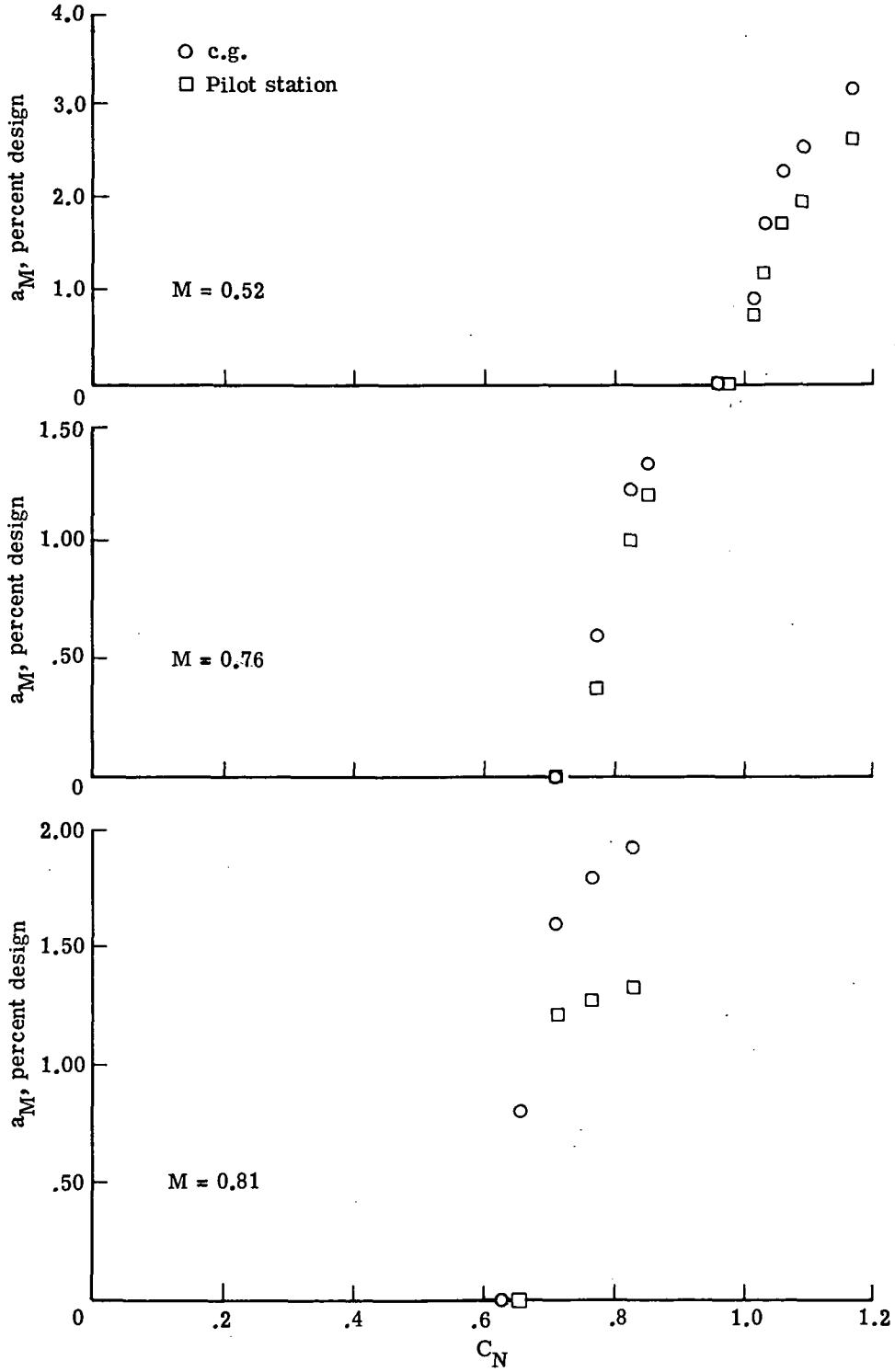

(a) Wing sweep angle, 26°.

Figure 11.- Comparisons of model buffet accelerations at center of gravity and pilot station normalized by design acceleration.

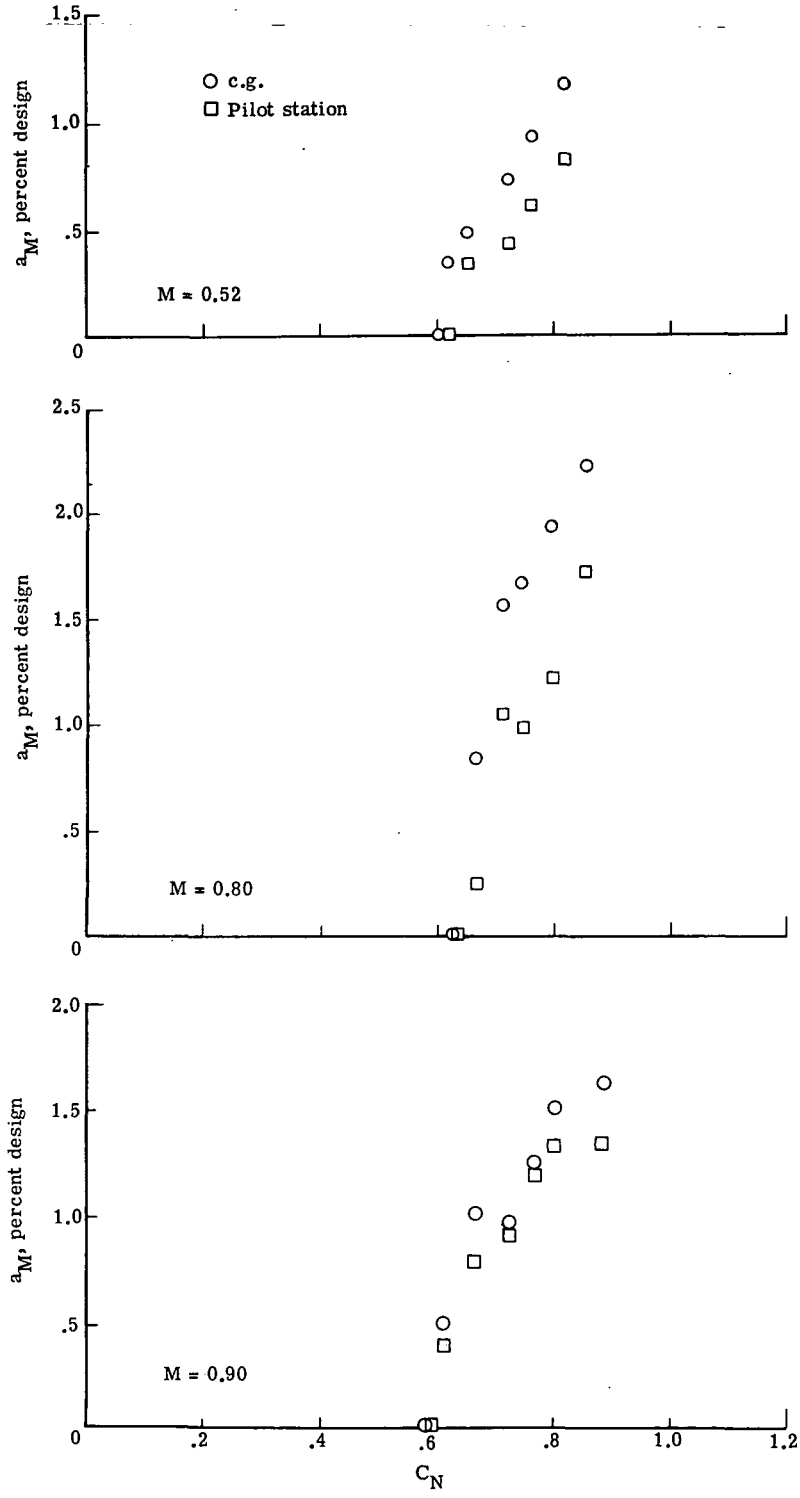

(b) Wing sweep angle, 50°.

Figure 11.- Continued.

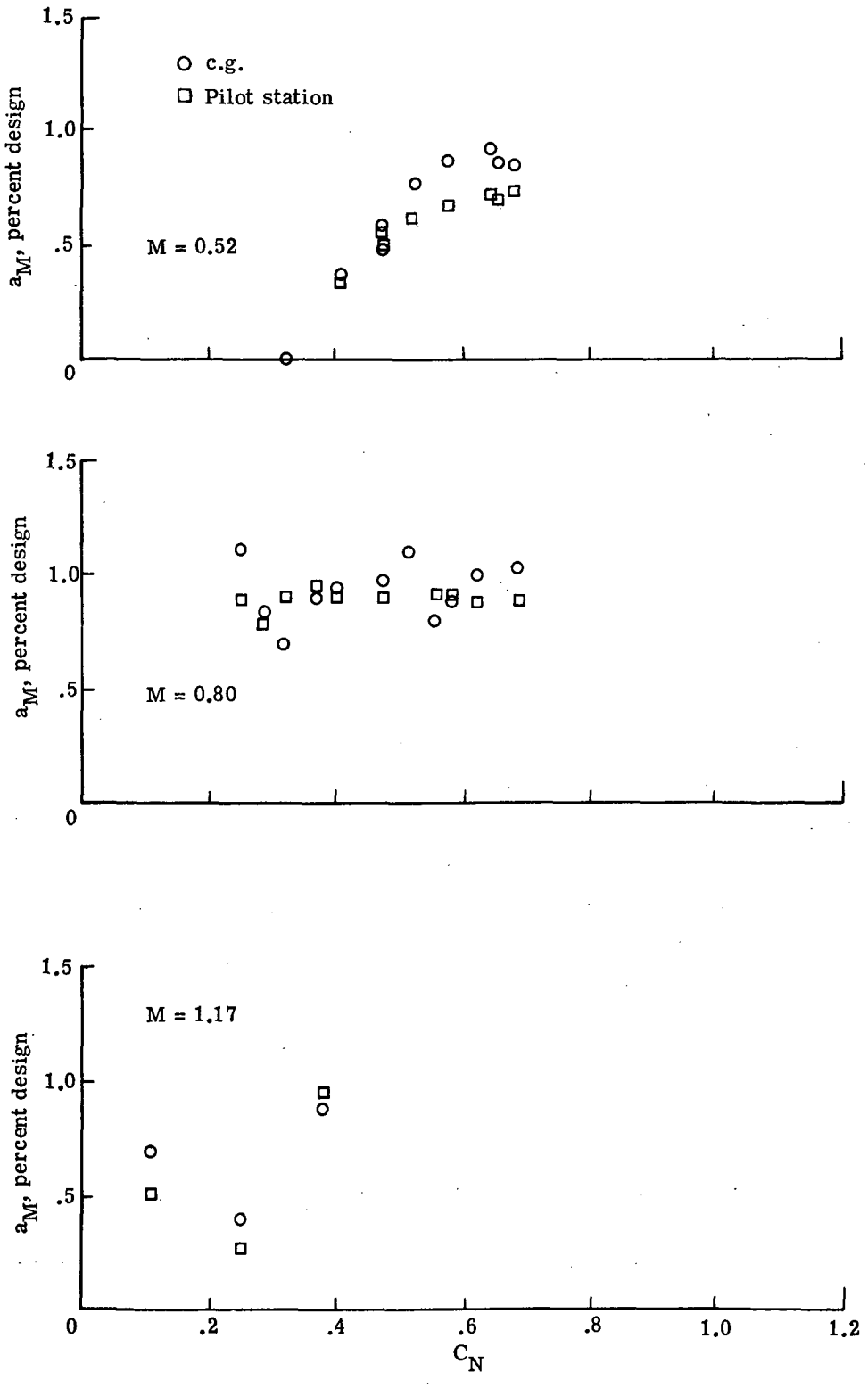

(c) Wing sweep angle, 72°.

Figure 11.- Concluded.

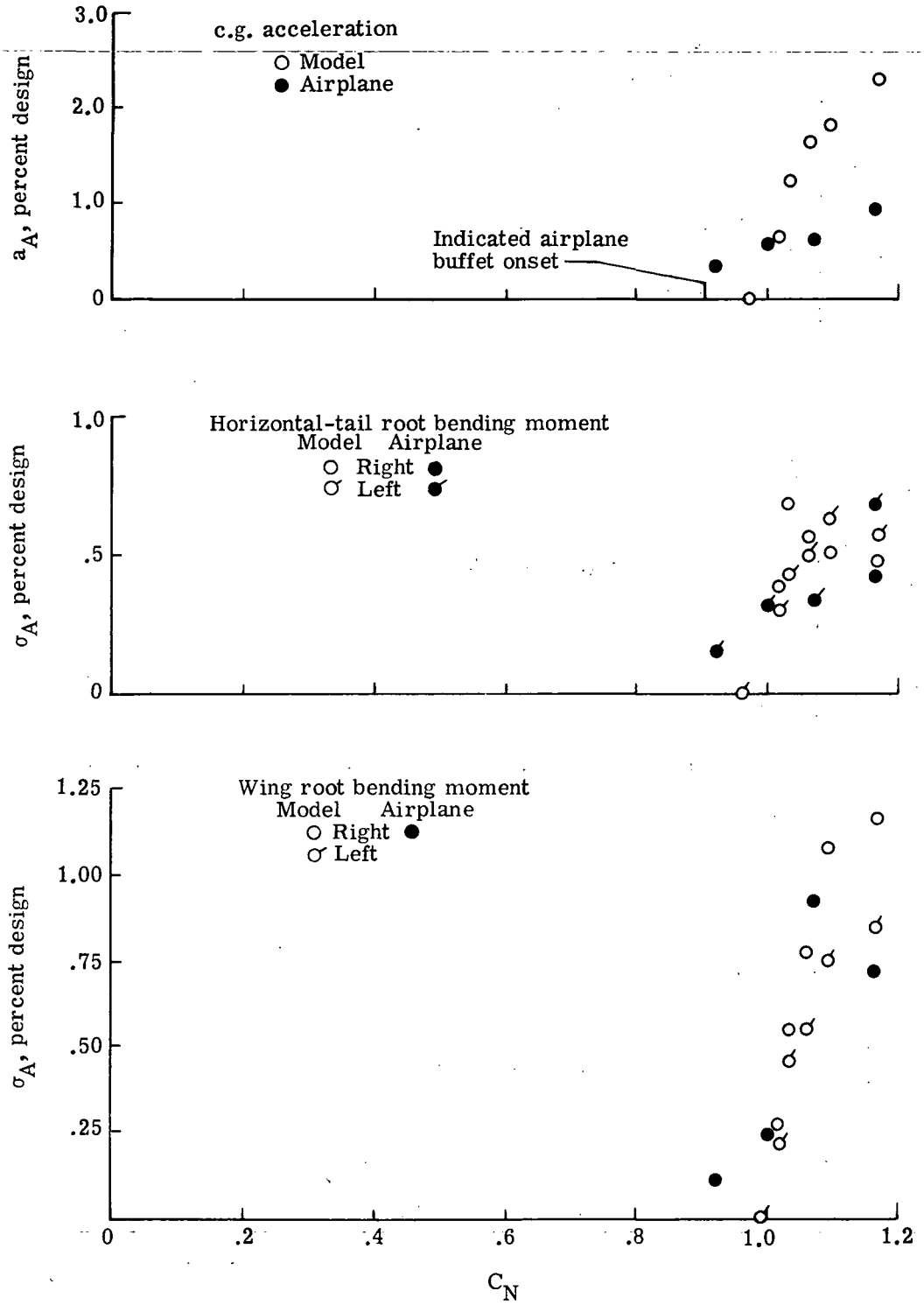

(a) $\Lambda = 26^{o}$; $M_M = 0.52$; $M_A = 0.53$ to 0.49.

Figure 12.- Comparison of airplane buffet response and buffet response predicted from model data normalized on airplane design loads.

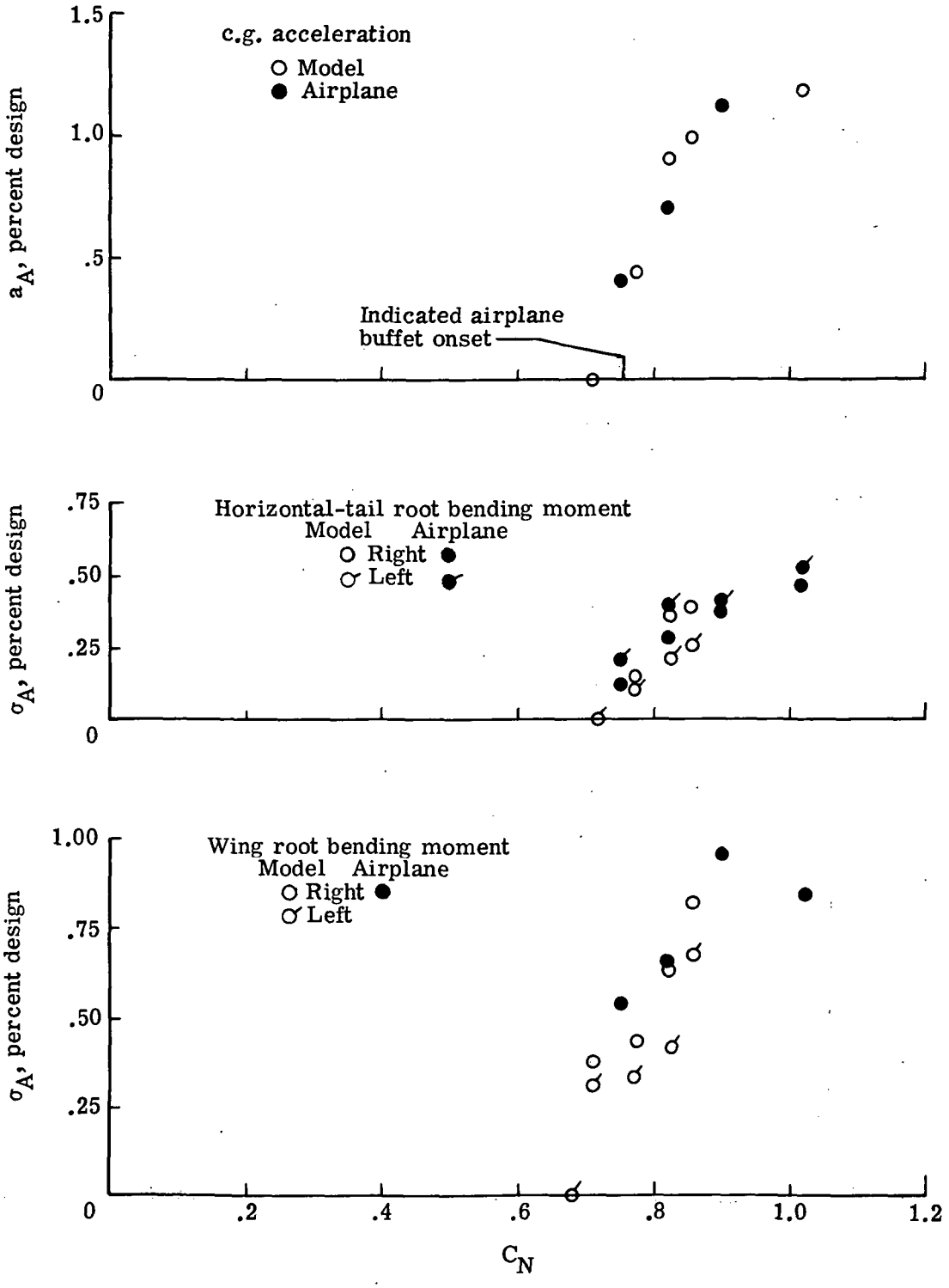

(b) $\Lambda = 26^{\circ}$; $M_M = 0.76$; $M_A = 0.76$ to 0.75.

Figure 12.- Continued.

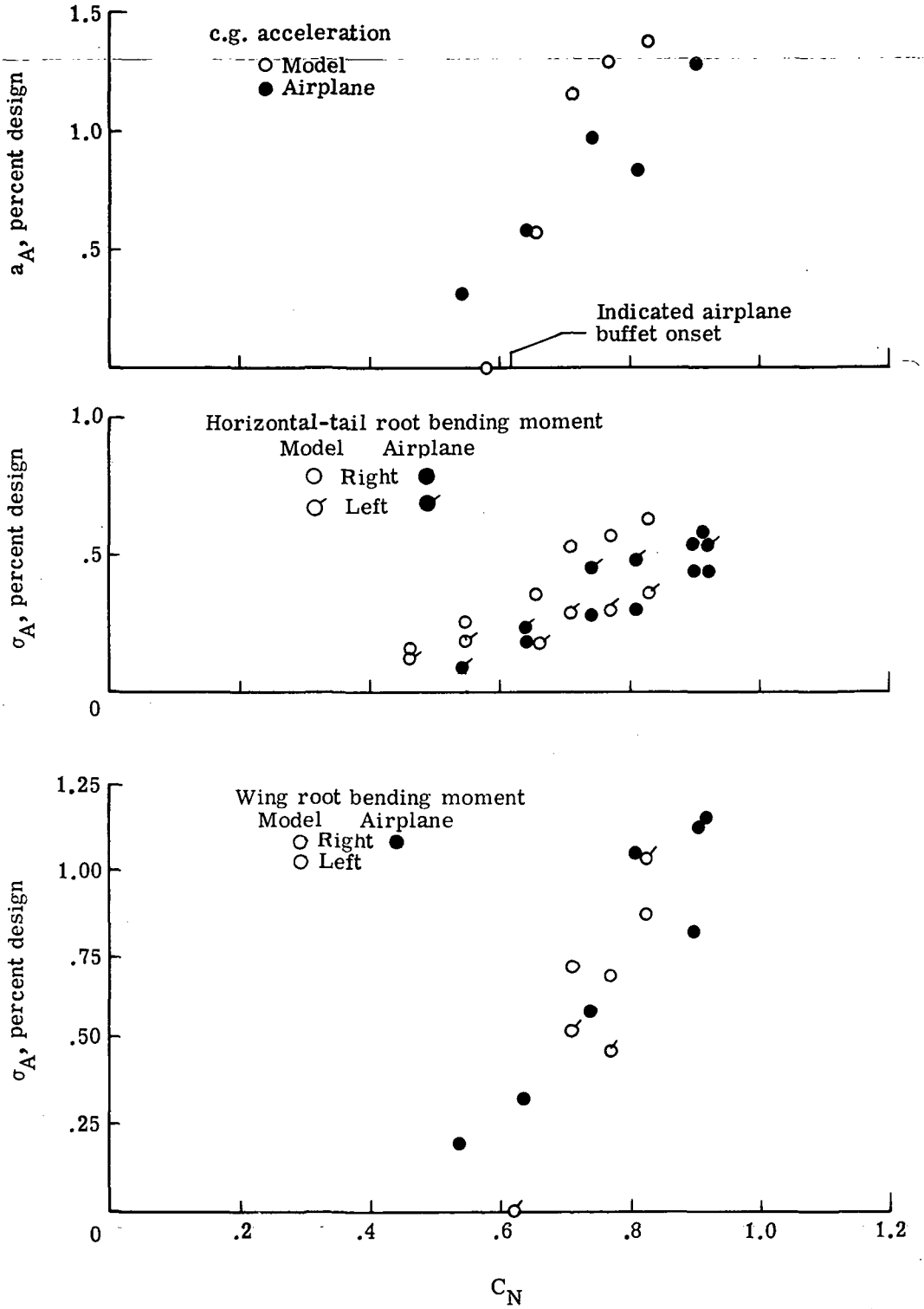

(c) $\Lambda = 26^{o}$; $M_M = 0.81$; $M_A = 0.83$ to 0.81.

Figure 12.- Continued.

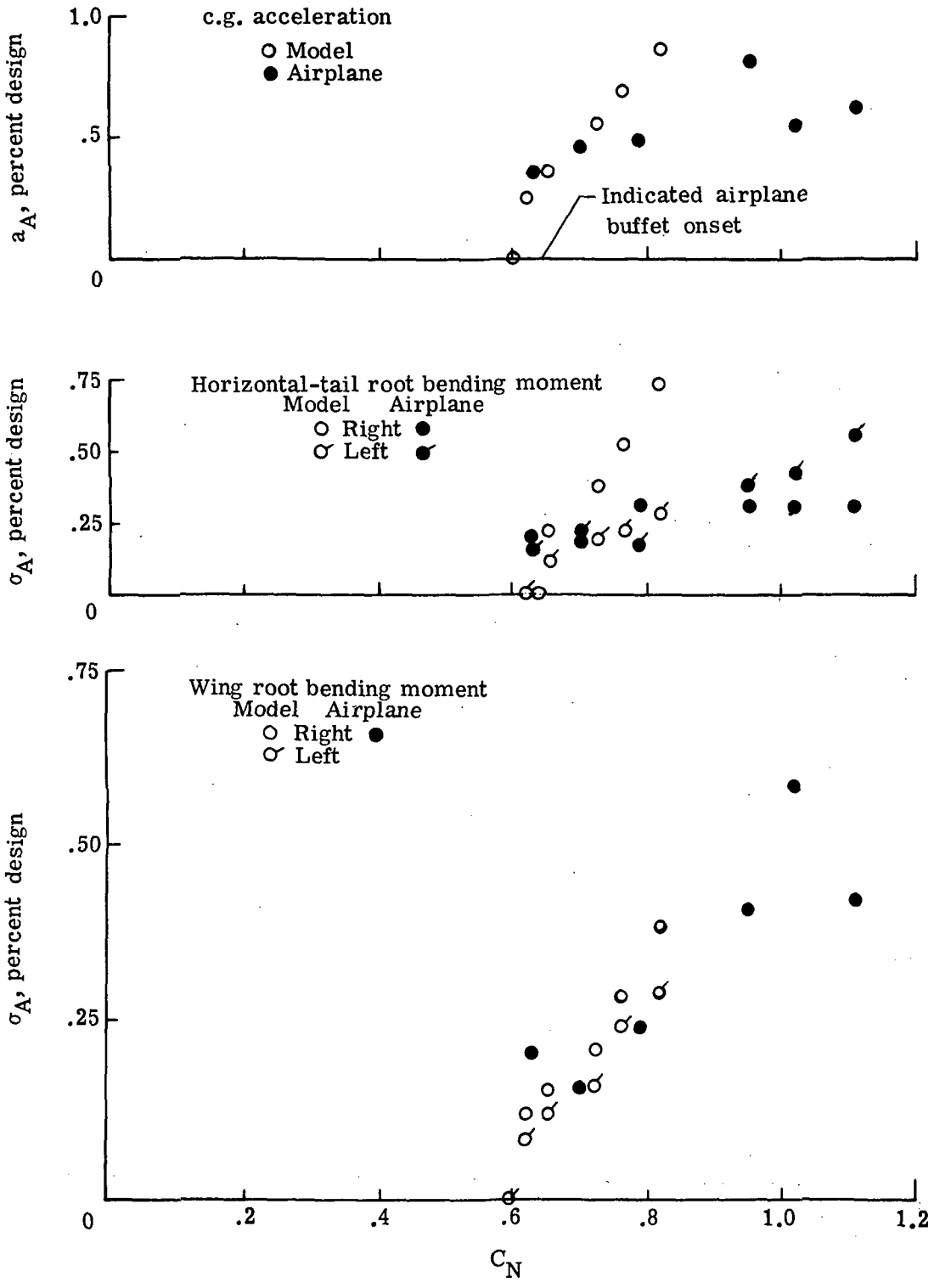

(d) $\Lambda = 50^{o}$; $M_M = 0.52$; $M_A = 0.53$ to 0.48.

Figure 12.- Continued.

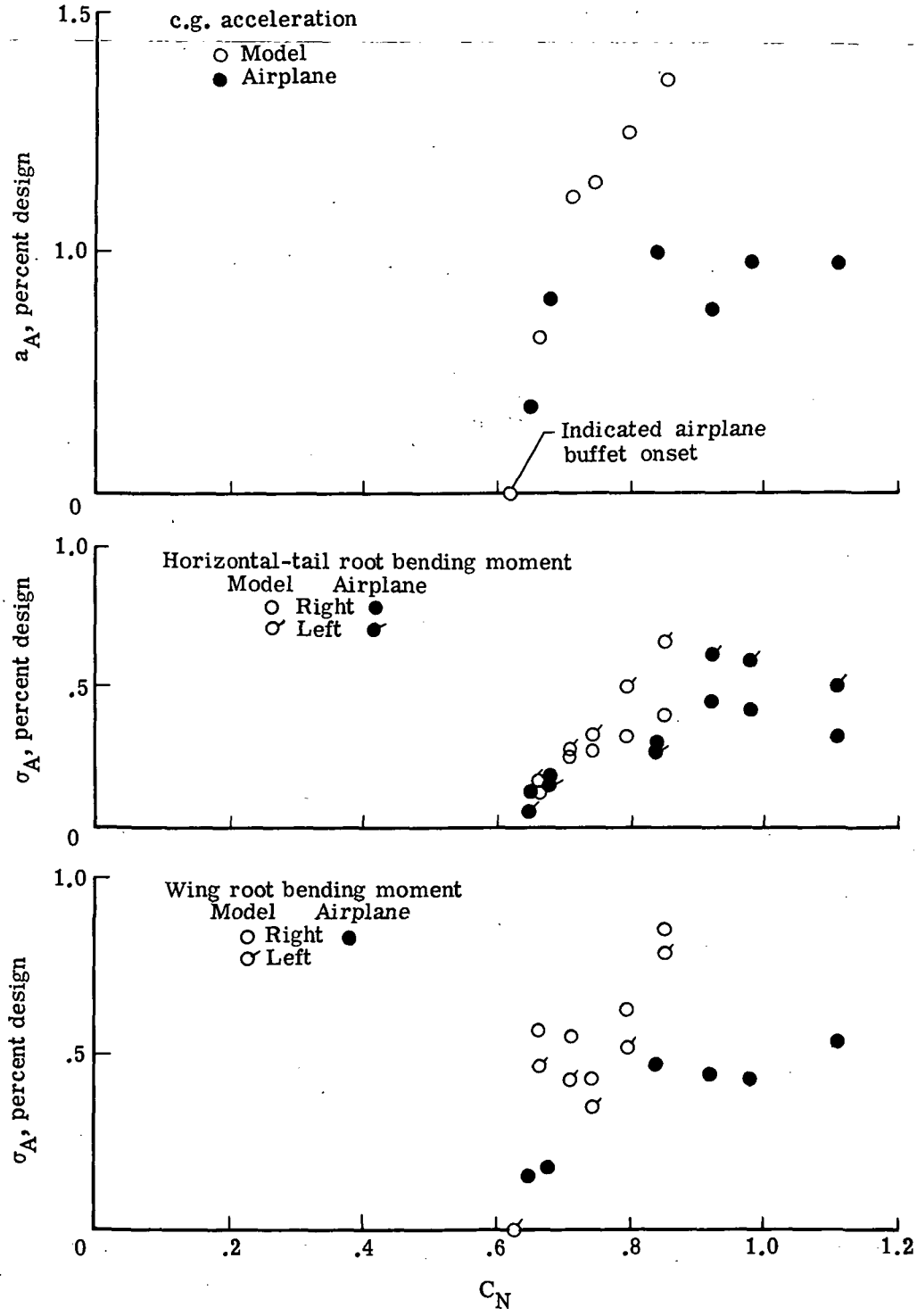

(e) $\Lambda = 50^{\circ}$; $M_M = 0.80$; $M_A = 0.81$ to 0.73.

Figure 12.- Continued.

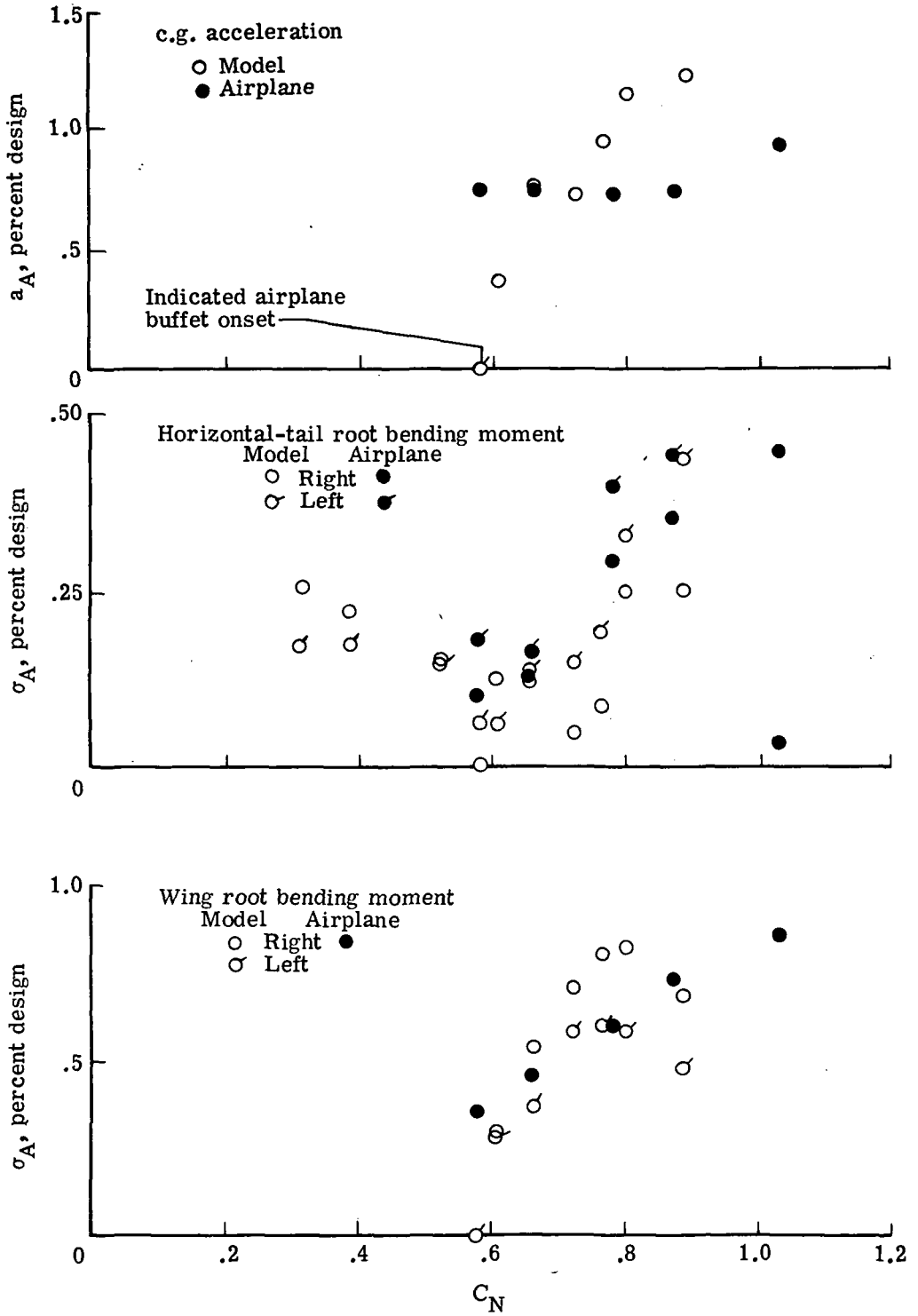

(f) $\Lambda = 50^o$; $M_M = 0.90$; $M_A = 0.95$ to 0.89.

Figure 12.- Continued.

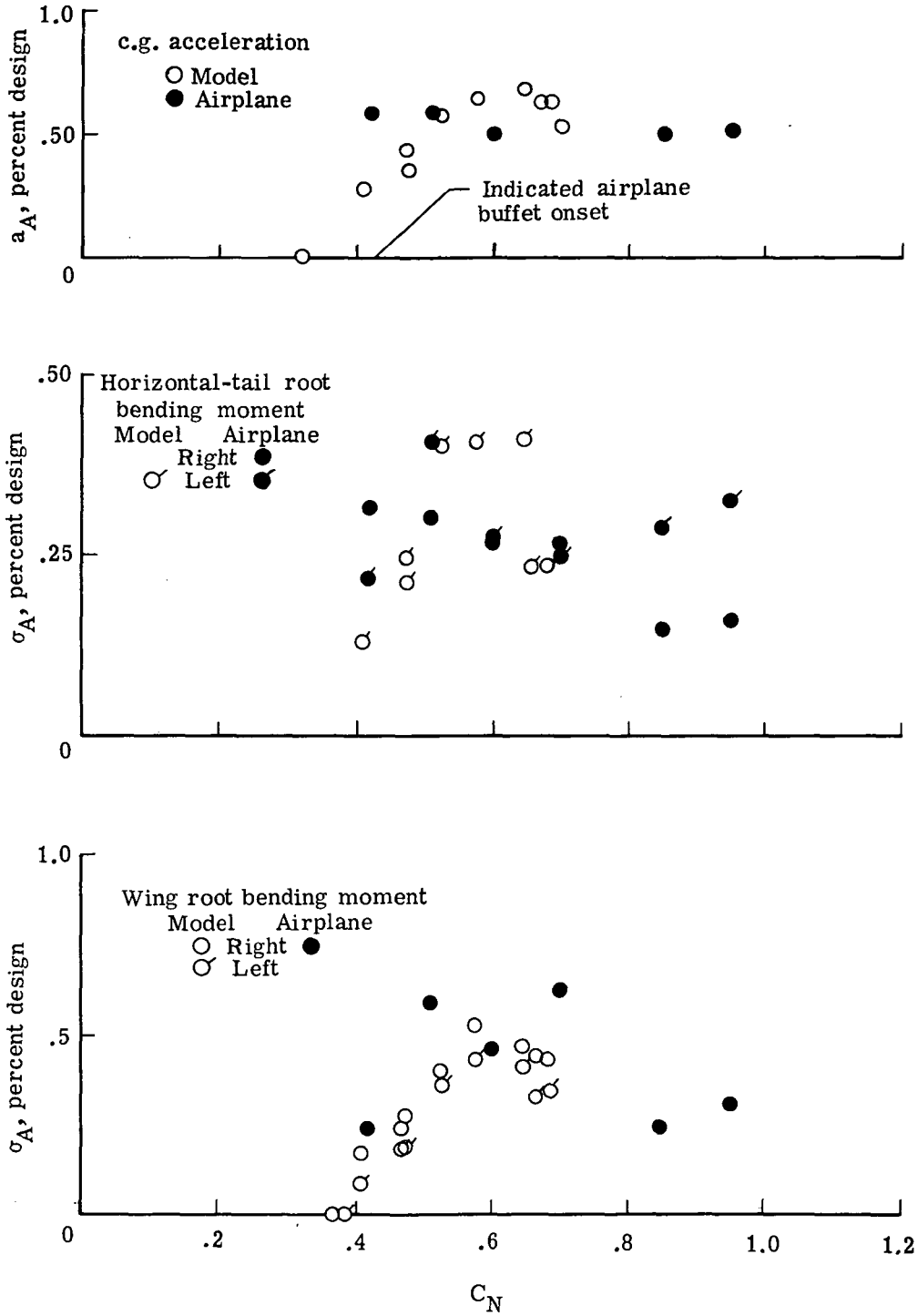

(g) $\Lambda = 72^{o}$; $M_M = 0.52$; $M_A = 0.56$ to 0.51.

Figure 12.- Continued.

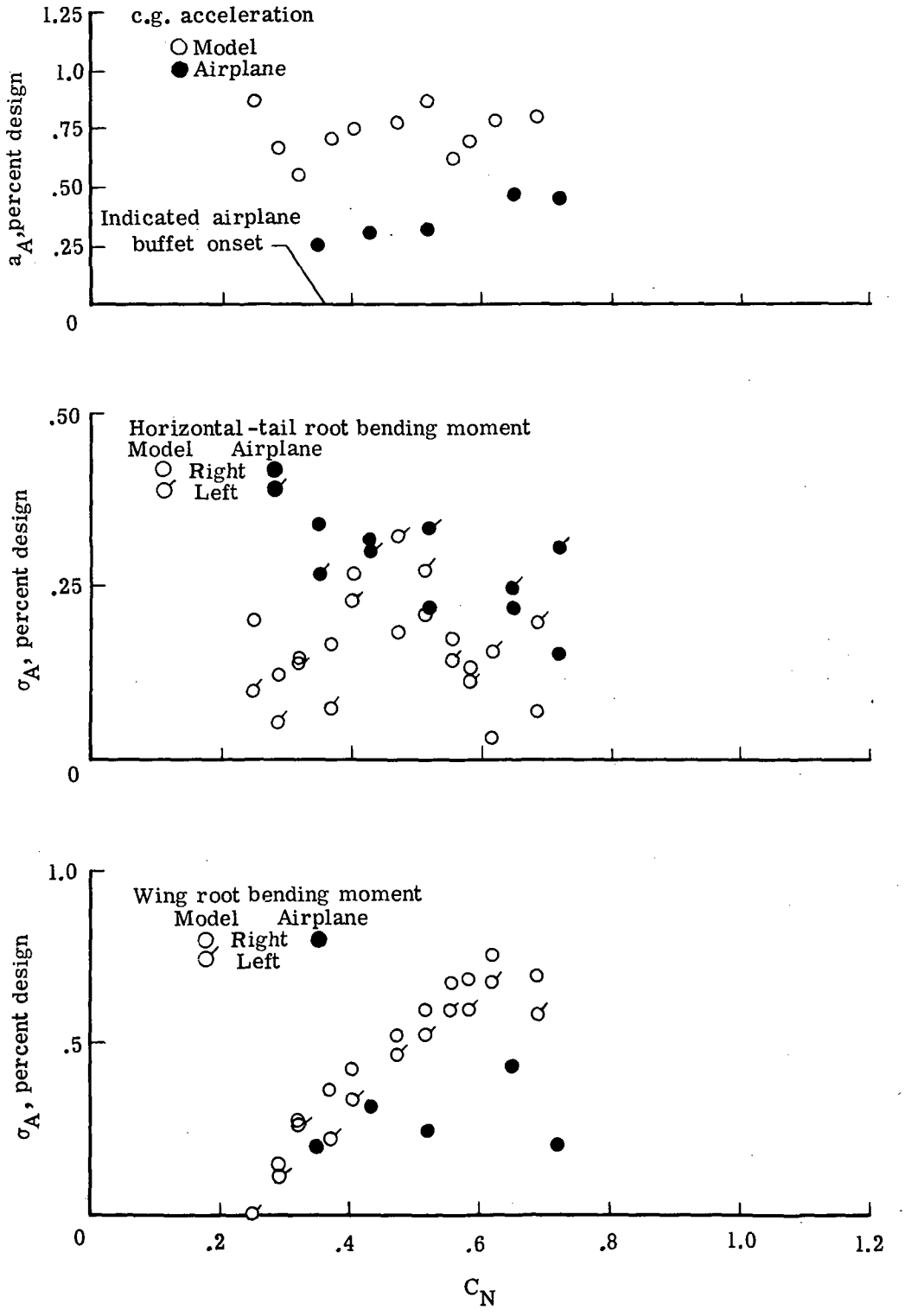

(h) $\Lambda = 72^{\circ}$; $M_M = 0.80$; $M_A = 0.81$ to 0.76.

Figure 12.- Continued.

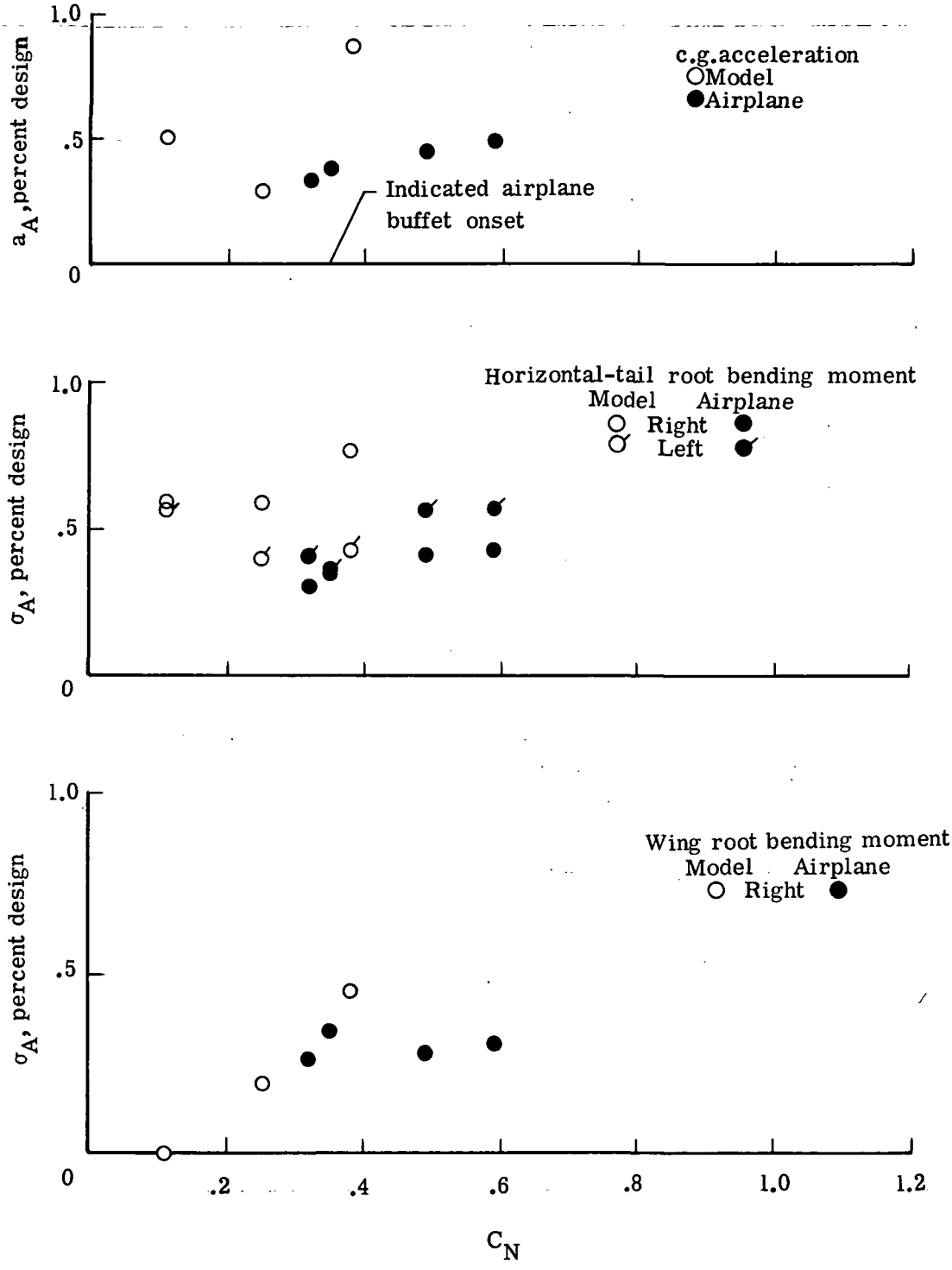

(i) $\Lambda = 72^{\circ}$; $M_M = 1.17$; $M_A = 1.23$ to 1.16.

Figure 12.- Concluded.

NASA-Langley, 1973 — 32 L-8460

"The aeronautical and space activities of the United States shall be conducted so as to contribute . . . to the expansion of human knowledge of phenomena in the atmosphere and space. The Administration shall provide for the widest practicable and appropriate dissemination of information concerning its activities and the results thereof."

—NATIONAL AERONAUTICS AND SPACE ACT OF 1958

NASA SCIENTIFIC AND TECHNICAL PUBLICATIONS

TECHNICAL REPORTS: Scientific and technical information considered important, complete, and a lasting contribution to existing knowledge.

TECHNICAL NOTES: Information less broad in scope but nevertheless of importance as a contribution to existing knowledge.

TECHNICAL MEMORANDUMS: Information receiving limited distribution because of preliminary data, security classification, or other reasons. Also includes conference proceedings with either limited or unlimited distribution.

CONTRACTOR REPORTS: Scientific and technical information generated under a NASA contract or grant and considered an important contribution to existing knowledge.

TECHNICAL TRANSLATIONS: Information published in a foreign language considered to merit NASA distribution in English.

SPECIAL PUBLICATIONS: Information derived from or of value to NASA activities. Publications include final reports of major projects, monographs, data compilations, handbooks, sourcebooks, and special bibliographies.

TECHNOLOGY UTILIZATION PUBLICATIONS: Information on technology used by NASA that may be of particular interest in commercial and other non-aerospace applications. Publications include Tech Briefs, Technology Utilization Reports and Technology Surveys.

Details on the availability of these publications may be obtained from:

SCIENTIFIC AND TECHNICAL INFORMATION OFFICE

NATIONAL AERONAUTICS AND SPACE ADMINISTRATION

Washington, D.C. 20546